U.S. DEPARTMENT OF COMMERCE

PB80-175276

# Emissions Correlations for Conventional Gas Turbines

Purdue Univ, Lafayette, IN

Prepared for

Environmental Protection Agency
Ann Arbor, MI

Dec 77

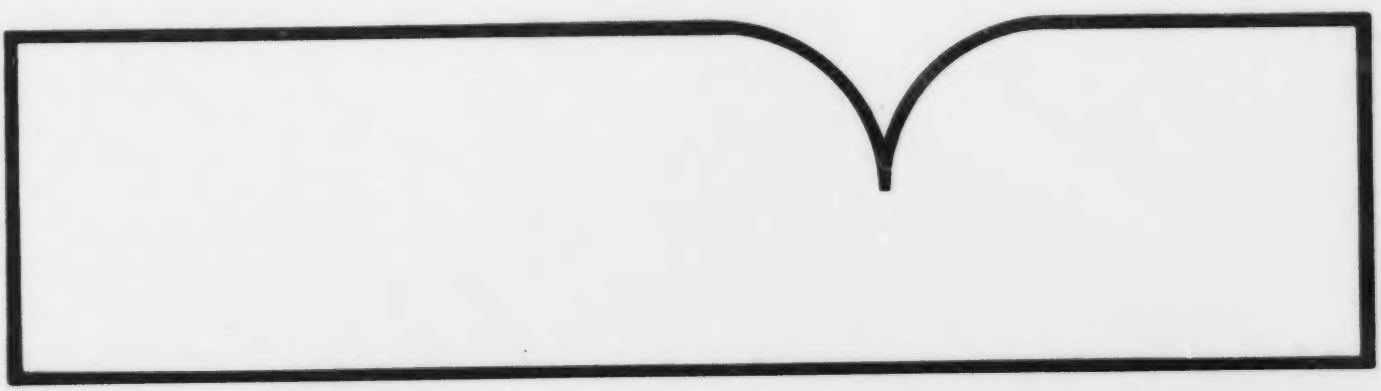

U.S. Department of Commerce
National Technical Information Service
NTIS.

PB80-175276

# EMISSIONS CORRELATIONS FOR CONVENTIONAL GAS TURBINES

## Environmental Protection Agency Grant No. R-804443-01-Final Report

by

R. M. Washam and A. M. Mellor

Report No. PURDU-CL-77-06

THE COMBUSTION LABORATORY
SCHOOL OF MECHANICAL ENGINEERING
PURDUE UNIVERSITY
WEST LAFAYETTE, INDIANA

December 1977

REPRODUCED BY
NATIONAL TECHNICAL
INFORMATION SERVICE
U.S. DEPARTMENT OF COMMERCE
SPRINGFIELD, VA. 22161

**TECHNICAL REPORT DATA**
*(Please read Instructions on the reverse before completing)*

| | | |
|---|---|---|
| 1. REPORT NO.<br>PURDU-CL-77-06 | 2. | 3. RECIPIENT'S ACCESSION NO.<br>PB 80 175276 |
| 4. TITLE AND SUBTITLE<br>Emissions Correlations for Conventional Gas Turbines | | 5. REPORT DATE<br>December 1977<br>6. PERFORMING ORGANIZATION CODE |
| 7. AUTHOR(S)<br>R.M. Washam<br>A.M. Mellor | | 8. PERFORMING ORGANIZATION REPORT NO. |
| 9. PERFORMING ORGANIZATION NAME AND ADDRESS<br>The Combustion Laboratory<br>School of Mechanical Engineering<br>Purdue University<br>West Lafayette, Indiana | | 10. PROGRAM ELEMENT NO.<br>11. CONTRACT/GRANT NO.<br>R-804443-01-Final Report |
| 12. SPONSORING AGENCY NAME AND ADDRESS<br>U.S. Environmental Protection Agency | | 13. TYPE OF REPORT AND PERIOD COVERED<br>Final Report<br>14. SPONSORING AGENCY CODE |

15. SUPPLEMENTARY NOTES

16. ABSTRACT

The production of gaseous pollutants from conventional gas turbine combustors is being investigated through the use of a characteristic time model. Here, the dominant subprocesses (liquid fuel evaporation, turbulent mixing, and chemical reaction) affecting the formation and destruction of pollutant species are expressed in terms of times and then sums and ratios of these times are used to correlate emissions.

Correlations are done for combustors of three engines (the General Motors GT-309, the Detroit Diesel Allison T-63, and the Pratt and Whitney JT9D); the model predicts the effect of combustor geometry, fuel type, power level, ambient conditions, etc. on the levels of pollutants produced. In addition, the model shows promise as an emissions optimization tool as demonstrated for the GT-309. And, there are indications that, for specific pollutants, universal correlations for all conventional gas turbine combustors can be performed with the model. Generally heterogeneous effects are ignored.

17. KEY WORDS AND DOCUMENT ANALYSIS

| a. DESCRIPTORS | b. IDENTIFIERS/OPEN ENDED TERMS | c. COSATI Field/Group |
|---|---|---|
| Air Pollution<br>Gas Turbine Engine<br>Emission<br>Exhaust Gases<br>Correlations | Gas Turbine Combustors | |

| | | |
|---|---|---|
| 18. DISTRIBUTION STATEMENT<br>RELEASE UNLIMITED | 19. SECURITY CLASS *(This Report)*<br>UNCLASSIFIED<br>20. SECURITY CLASS *(This page)*<br>UNCLASSIFIED | 21. NO. OF PAGES<br>22. PRICE |

EPA Form 2220-1 (9-73)

# EMISSIONS CORRELATIONS FOR CONVENTIONAL GAS TURBINES

Environmental Protection Agency
Grant No. R-804443-013 - Final Report

by
R. M. Washam and A. M. Mellor

Report No. PURDU-CL-77-06
The Combustion Laboratory
School of Mechanical Engineering
Purdue University
West Lafayette, Indiana

December, 1977

## ACKNOWLEDGEMENTS

The authors acknowledge Dr. J. H. Tuttle of General Motors Research Laboratories and Dr. M. B. Colket of United Technologies Research Center for their assistance with calculations for the T-63 combustor analysis while at Purdue University. Also we are grateful for the cooperation of Mr. A. W. Nelson and Dr. G. Sturgess of Pratt and Whitney Aircraft in obtaining data for the JT9D combustor. Prof. S. J. Citron of Purdue provided consulting in programming; Mr. D. Ramsey; also of Purdue, was particularly valuable in calculating exhaust and flame temperatures.

Financial support for this research was provided by the Environmental Protection Agency under Grant Number R-804443. The contents do not necessarily reflect the views and policies of the Environmental Protection Agency, nor does mention of trade names or commercial products constitute endorsement or recommendation. Finally, we appreciate Dr. R. Munt for his support as grant monitor.

TABLE OF CONTENTS

Page

LIST OF TABLES. . . . . .v

LIST OF FIGURES . . . . . .vi

ABSTRACT. . . . . .viii

SECTION I. INTRODUCTION . . . . . .1

SECTION II. CHARACTERISTIC TIMES . . . . . .4

A. Heterogeneous Processes . . . . . .5

B. Mixing Processes. . . . . .7

C. Chemical Processes. . . . . .9

D. Derivation of Characteristic Time Ratios. . . . . .12

E. Summary . . . . . .14

SECTION III. CHARACTERISTIC TIME STUDIES ON THE GT-309 COMBUSTOR . . . . . .15

A. Sample Optimization . . . . . .16

B. Current GT-309 Correlation. . . . . .23

C. Summary . . . . . .29

SECTION IV. CHARACTERISTIC TIME STUDIES ON THE T-63 COMBUSTOR . . . . . .31

A. $NO_X$EI Correlation . . . . . .35

B. COEI Correlation. . . . . .39

C. HCEI Correlation. . . . . .41

D. Advanced Combustors . . . . . .43

E. Summary . . . . . .46

Page

SECTION V. CHARACTERISTIC TIME STUDIES ON THE JT9D COMBUSTOR. . . . . .47

A. Nitric Oxides Correlation . . . . . .47

B. Carbon Monoxide Correlation . . . . . .51

C. Ambient Effects on Nitric Oxides. . . . . .53

D. Summary . . . . . .66

SECTION VI. CONCLUSIONS. . . . . .67

A. Nitric Oxides . . . . . .67

B. Carbon Monoxide . . . . . .69

C. Summary . . . . . .71

LIST OF REFERENCES. . . . . .72

LIST OF TABLES


| Table | | Page |
|---|---|---|
| 2-1 | Characteristic Times for Combustion and Pollutant Formation in Two-Phase Turbulent Flow (from Mellor, 1976). . . . . | 5 |
| 3-1 | Quench Length for the GT-309 Carbon Monoxide Correlation . . . . . | 29 |
| 4-1 | T-63 Combustor Operating Conditions (Troth et al., 1973) and Computed Chemical Kinetic Times (JP4 Fuel) . . . . . | 32 |
| 4-2 | T-63 Combustor Operating Conditions (Moses, 1975) and Computed Chemical Kinetic Times. . . . . | 33 |
| 4-3 | T-63 $NO_2$ Emissions (Moses, 1976) . . . . . | 35 |
| 4-4 | Macroscales for T-63 NO and CO Emissions . . . . . | 38 |
| 5-1 | Temperatures Calculated with Measured Inlet Conditions (.0073 g $H_2O$/g air) . . . . . | 56 |
| 5-2 | Temperatures Calculated Assuming Zero Humidity . . . . . | 59 |
| 5-3 | Baseline Temperatures, Engine P896, Computed with Measured Inlet Conditions (294°K, 0.99 atm). . . . . | 60 |
| 5-4 | Temperatures, Engine P896, Computed for 244°K, 0.99 atm. . . . . | 61 |
| 5-5 | Temperatures, Engine P896, Computed for 322°K, 0.99 atm. . . . . | 61 |
| 5-6 | Temperatures, Engine P896, Computed for 294°K, 0.95 atm. . . . . | 63 |
| 5-7 | Temperatures, Engine P896, Computed for 294°K, 1.05 atm. . . . . | 63 |
| 6-1 | Constants for $NO_xEI = A\tau_{s\ell,no}/\tau_{no} + B$. . . . . | 67 |
| 6-2 | Constants for $COEI = C\tau_{co}/\tau_{s\ell,co} + D$ . . . . . | 71 |

LIST OF FIGURES


| Figure | | Page |
|---|---|---|
| 1-1. | Correlation of $NO_X$EI with combustor inlet air temperature (from Lipfert, 1972) | 2 |
| 2-1 | Typical gas turbine combustor flow schematic | 6 |
| 2-2 | Schematic of postulated primary and secondary zone flow pattern for the J-33 combustor (from Mellor et al., 1972 and Tuttle et al., 1973) | 8 |
| 2-3 | Correlation of $NO_X$EI with stoichiometric adiabatic flame temperature, based on combustor inlet air temperature (from Sawyer et al., 1973) | 11 |
| 3-1 | Variation of $NO_X$EI and COEI with combustor geometry at 90% power point (from Tuttle et al., 1976) | 17 |
| 3-2 | Variation of $NO_X$EI and COEI with combustor geometry at 60% power point (from Tuttle et al., 1976) | 18 |
| 3-3 | GT-309 combustor geometries (from Hammond, 1977) | 19 |
| 3-4 | Comparison of predicted and experimental EI($NO_X$) vs. gasifier speed (from Hammond, 1977) | 21 |
| 3-5 | Comparison of predicted and experimental EI(CO) vs. gasifier speed (from Hammond, 1977) | 22 |
| 3-6 | Correlation of the GT-309 $NO_X$EI data | 25 |
| 3-7 | Correlation of the GT-309 $NO_X$EI data assuming reversing flow | 26 |
| 3-8 | Correlation of the GT-309 COEI data. | 28 |
| 4-1 | The T-63 baseline burner geometry. | 34 |
| 4-2 | Correlation of the T-63 (conventional burners) $NO_X$EI data. | 37 |
| 4-3 | Correlation of the T-63 (conventional burners) COEI data | 40 |
| 4-4 | Correlation of T-63 HCEI data. | 42 |
| 4-5 | $NO_X$EI for advanced T-63 combustors | 44 |

| Figure | | Page |
|---|---|---|
| 4-6 | COEI for advanced T-63 combustors. . . . . | .45 |
| 5-1 | Half-section of the JT9D combustor . . . . . | .48 |
| 5-2 | Correlation of the JT9D $NO_x$EI data . . . . . | .50 |
| 5-3 | Correlation of the JT9D COEI data. . . . . | .52 |
| 5-4 | Correlation of the JT9D $NO_x$EI data for one burner modification with one fuel. . . . . | .55 |
| 5-5 | Correlation of the JT9D $NO_x$EI data for one burner modification with one fuel and neglecting ambient humidity. . . . . | .57 |
| 5-6 | Ambient temperature effect on $NO_x$EI. . . . . | .62 |
| 5-7 | Ambient pressure effect on $NO_x$EI . . . . . | .64 |
| 6-1 | $NO_x$EI correlation for three engines. . . . . | .68 |
| 6-2 | COEI correlation for three engines . . . . . | .70 |

## ABSTRACT

The production of gaseous pollutants from conventional gas turbine combustors is being investigated through the use of a characteristic time model. Here, the dominant subprocesses (liquid fuel evaporation, turbulent mixing, and chemical reaction) affecting the formation and destruction of pollutant species are expressed in terms of times and then sums and ratios of these times are used to correlate emissions.

Correlations are done for combustors of three engines (the General Motors GT-309, the Detroit Diesel Allison T-63, and the Pratt and Whitney JT9D); the model predicts the effect of combustor geometry, fuel type, power level, ambient conditions, etc. on the levels of pollutants produced. In addition, the model shows promise as an emissions optimization tool as demonstrated for the GT-309. And, there are indications that, for specific pollutants, universal correlations for all conventional gas turbine combustors can be performed with the model. Generally heterogeneous effects are ignored.

# I. INTRODUCTION

Gas turbine engines are devices that convert heat into mechanical energy or thrust: the mechanical energy is usually a driven shaft and the thrust is used to propel a vehicle. The heat is the result of the conversion of chemical bond energy into sensible enthalpy; this process occurs in the gas turbine combustor. Here, for our purposes, a liquid fuel is introduced into the combustor, evaporates, and burns. This elevates the temperature of the flow which then is used to produce power. The combustor's flame is stabilized inside of a liner with sizes and placements of the air addition holes determining the flow pattern, and thus affecting the flame structure.

In recent years there has been a growing concern about the effect of our technology on the quality of the environment. Along this line, gas turbines are known to produce a variety of gaseous pollutant emissions; this report is concerned with a technique to correlate, predict, and optimize emissions from these devices. Specifically, we are interested in nitric oxides, carbon dioxide, and unburned hydrocarbons.

In the past, emissions from gas turbines have been correlated versus a variety of variables: pressure, fuel type, humidity, etc. Fig. 1-1, from Lipfert (1972), shows a representative correlation of nitric oxides emission index (emission index: gram pollutant/kilogram fuel) in terms of combustor inlet temperature; notice that, for the engines shown, a single curve results. Therefore, knowing the combustor inlet temperature, a correlation of this type could be used to predict the amount of nitric oxides one of these engines would produce, but this correlation is not consistent for all engines. In this report, we present a correlating technique that may be able to produce a universal correlation for a specific emission from all conventional gas turbine combustors. This model, derived in Section II, has parameters composed of quantities either known, or available, to the combustion engineer; it can be used to predict how geometry variations, ambient conditions, etc., affect the level of pollutants produced. In this respect, it should have value as a design tool.

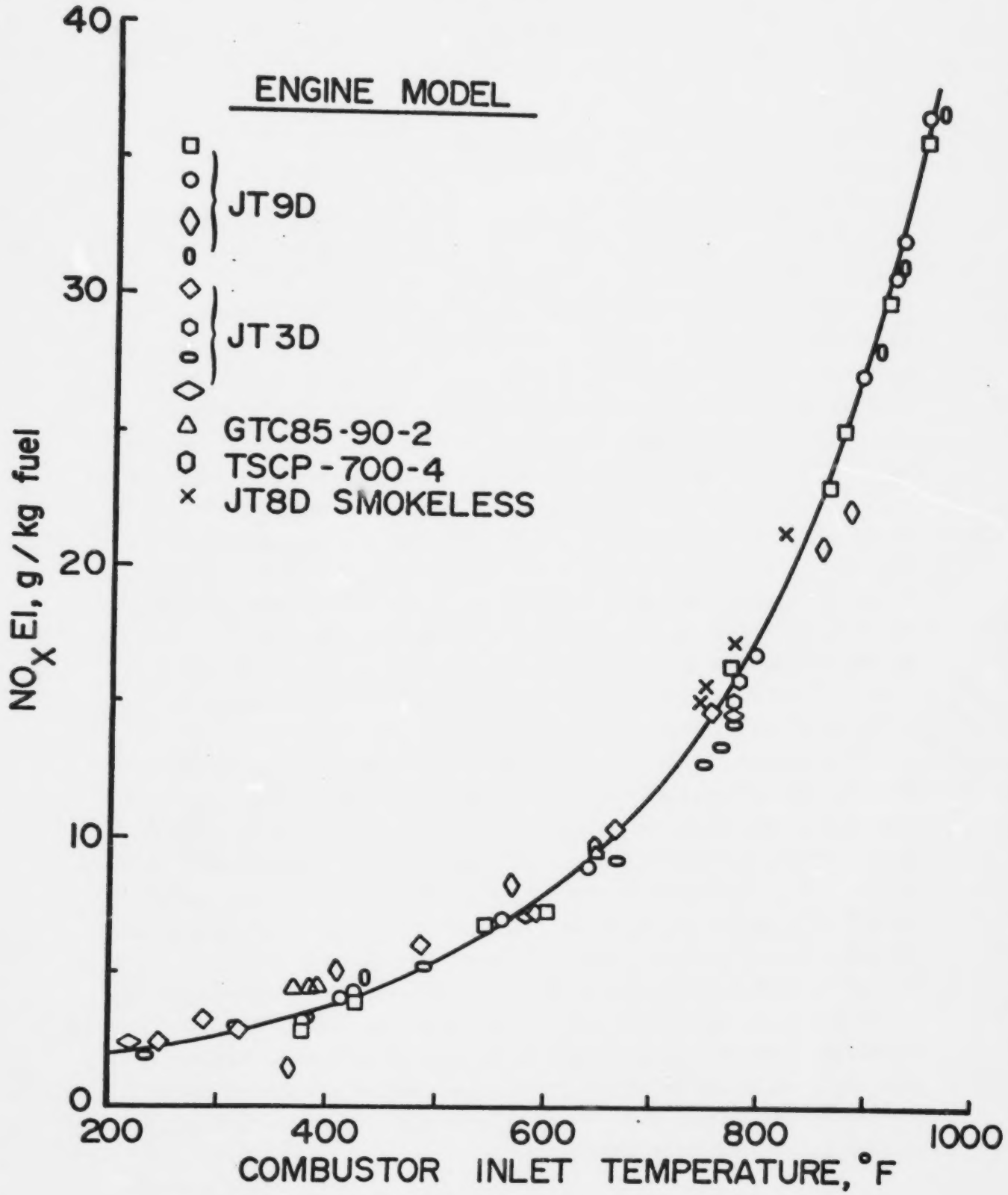


Figure 1-1. Correlation of $NO_X$EI with combustor inlet air temperature (from Lipfert, 1972).

Analyses of three gas turbine combustors follow. Emissions correlations for nitric oxides and carbon monoxide are performed for each combustor. In addition, Section III contains details of an emissions optimization test for the GT-309 auotmotive gas turbine which demonstrates the utility of the model for optimization work. The effects of advanced combustor designs on emissions are covered in Section IV. In Section V, ambient effects on nitric oxides from the JT9D combustor are investigated and a general prediction parameter is developed. Finally, data for all three combustors are correlated together in Section VI. If this is a universal correlation it should predict emissions levels for all conventional gas turbine burners.

## II. CHARACTERISTIC TIMES

The combustion process in liquid fuel spray flames is an extremely complex phenomenon. In conventional gas turbine burners, a turbulent, recirculating combustion zone is formed by the air flow pattern through the combustor liner. Also, this zone is two-phase since liquid fuel evaporates there, and the chemical composition is changing due to combustion.

In such flames, three dominant subprocesses must occur before combustion is complete. These are (1) evaporation of liquid fuel droplets, (2) mixing of fuel vapor with oxidizer to produce a combustible mixture, and (3) combustion of the resulting mixture. We seek to express these phenomenona in terms of characteristic times, and then use sums and ratios of these quantities to correlate engine emissions.

The characteristic times used are summarized in Table 2-1. The first time listed represents the lifetime of liquid fuel droplets. The duration of the lifetime is determined either by evaporation or by droplet combustion.

The second and third parameters in Table 2-1 characterize turbulent mixing processes. $\tau_{fi}$ is used for systems with air assist nozzles to account for mixing of fuel with the injecting air. The high velocity air flow through the nozzle shatters liquid fuel droplets, mixes fuel vapor with air, and adds oxidizer to the recirculation zone. The lifetime of the eddies in this region will affect the availability of suitable mixture for combustion.

$\tau_{s\ell}$ corresponds to the eddy dissipation time along the outer shear layer of the recirculation zone. In this region, the recirculating gases mix with fresh air flowing from the burner liner; these gases contain vaporized fuel that yields a combustible mixture when in the presence of suitable amounts of fresh air. Thus, the magnitude of $\tau_{s\ell}$ limits the extent of combustion in the flame zone.

$\tau_{co}$ and $\tau_{no}$ characterize the kinetic processes of homogeneous combustion. $\tau_{co}$ is the oxidation time for carbon monoxide. The magnitude of

this scale affects how complete combustion will be. $\tau_{no}$ is the time required for the formation of nitric oxide; the concentrations of nitric oxide formed will depend on the magnitude of this parameter. These times are functions of the local mixture ratio, the combustor pressure, and the local temperature of the respective regions of kinetic activity for each species.

Table 2-1. Characteristic Times for Combustion and Pollutant Formation in Two-Phase Turbulent Flow (from Mellor, 1976)

| Time | Symbol | Physical or Chemical Processes |
|---|---|---|
| Fuel droplet lifetime | $\tau_{eb}$ | Droplet evaporation and/or combustion |
| Eddy dissipation time for injected fluid | $\tau_{fi}$ | Small scale turbulent mixing near the fuel injector in the recirculation zone |
| Eddy dissipation time in the shear layer | $\tau_{s\ell}$ | Large scale turbulent mixing between fresh air and the recirculating burned gas - fuel mixture |
| Fuel ignition delay and burning time | $\tau_{hc}$ | Homogeneous combustion of the fuel to $CO_2$ |
| NO formation time | $\tau_{no}$ | Homogeneous kinetics for NO formation |

A. Heterogeneous Processes

From Mellor (1973), poor atomization of liquid fuel spray is known to increase the emission indices for CO, HC, and NO; therefore it is important to characterize this process in order to understand the heterogeneous effect on combustion. However, in the engines presented in this report the droplet effects are usually found to be negligible, but in order to be complete, a review of the effect follows.

The evaporation of liquid fuel droplets in conventional burners begins when the fuel is sprayed into the recirculation zone. Referring to Fig. 2-1, the recirculation zone is composed of hot burnt gases and the fuel spray. These hot burnt gases assist the evaporation of the fuel; because they are oxygen deficient, significant combustion does not take place.

The time required for vaporization affects the structure of the flame. While the size of the recirculation zone is principally a function of the design of the liner and the air addition velocities, long evaporation

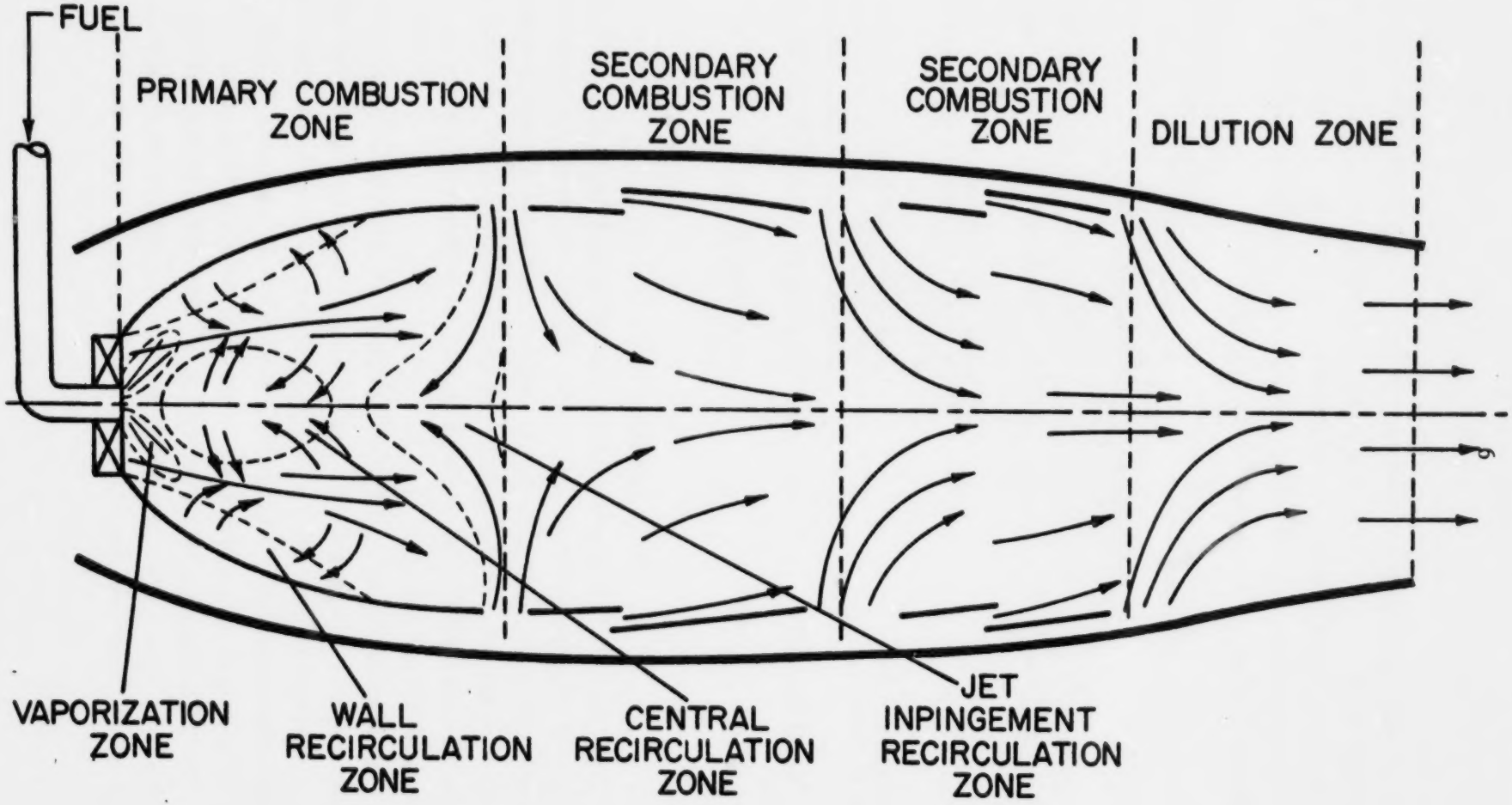


Figure 2-1. Typical gas turbine combustor flow schematic.

times can result in fuel droplets penetrating the shear layer and forming a free stream flame zone. In turn, this will affect the formation of pollutants. Fig. 2-1 illustrates this phenomenon.

For analysis purposes, the evaporation time is cast into the form

$$\tau_{eb} = d_i^2/\beta$$

The symbols are defined as follows:

$\tau_{eb}$: fuel droplet lifetime

$d_i$: initial droplet diameter

$\beta$: evaporation coefficient

The Sauter mean diameter is often used for the initial droplet diameter. The evaporation coefficient has units of length squared divided by time; a discussion of the determination of its value can be found in Mellor (1972).

## B. Mixing Processes

In general, air and fuel vapor must mix before combustion can take place. For a spray fueled combustor, this mixing is on the molecular level; therefore it must occur by molecular diffusion. The mixing is enhanced by turbulence.

Referring to Fig. 2-2, (from Mellor et al., 1972 and Tuttle et al., 1973), probing of an axisymmetric test combustor indicated that specific pollutant types tend to originate in different regions of the flame. The highest concentrations of CO and HC often are found in areas where the flame is quenched by the addition of colder air; for conventional burners, this is the portion of the shear layer affected by the flow from the air addition holes. The greatest concentrations of NO tend to be found in the area of highest temperature; for conventional burners, this is along the centerline downstream of the recirculation zone. Since CO and HC are often formed in different regions of the flame than those for NO, it is to be expected that the mixing times may be different for these pollutants.

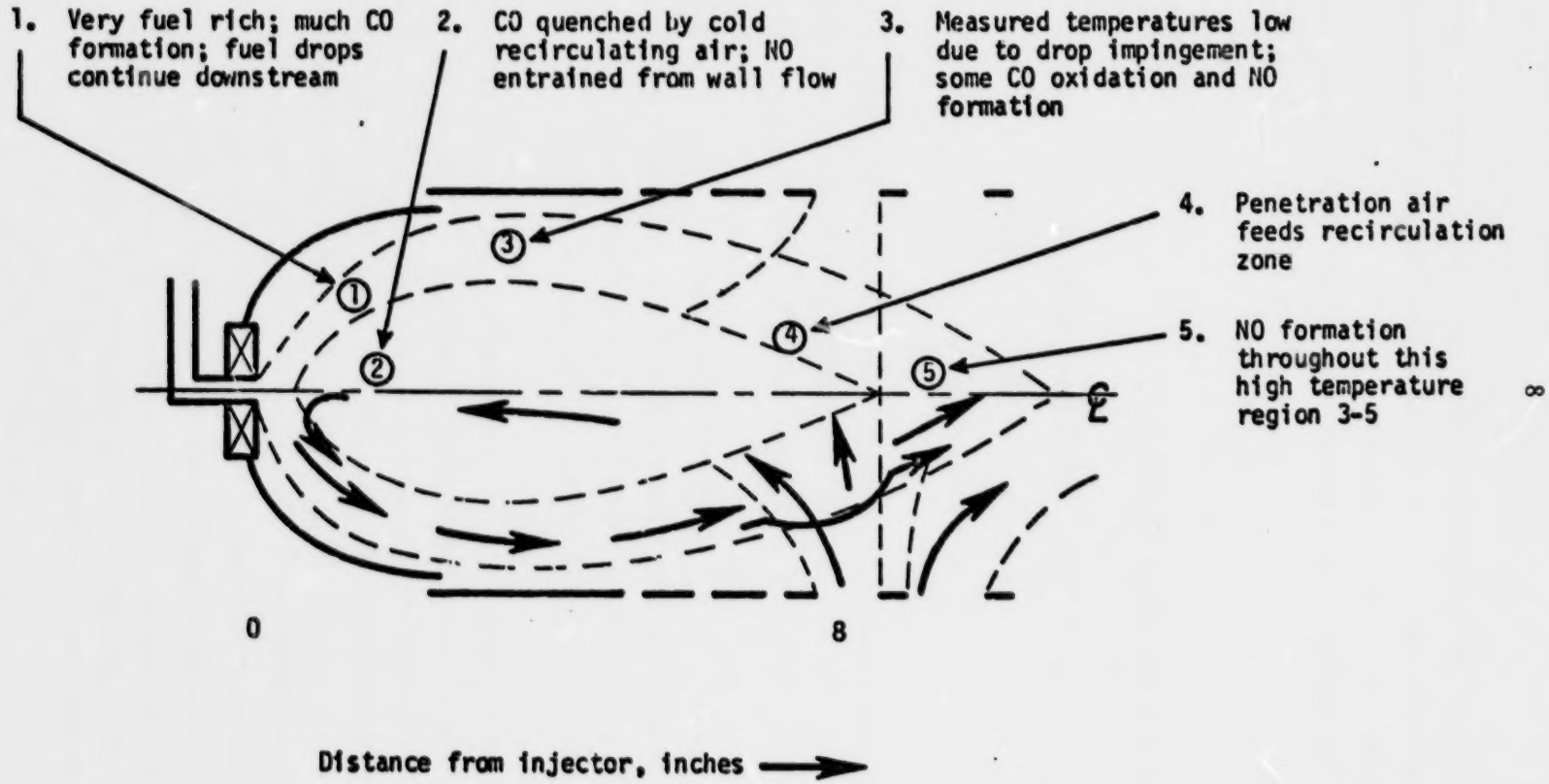
1. Very fuel rich; much CO formation; fuel drops continue downstream
2. CO quenched by cold recirculating air; NO entrained from wall flow
3. Measured temperatures low due to drop impingement; some CO oxidation and NO formation
4. Penetration air feeds recirculation zone
5. NO formation throughout this high temperature region 3-5
0
8
Distance from injector, inches

Figure 2-2. Schematic of postulated primary and secondary zone flow pattern for the J-33 combustor (from Mellor et al., 1972 and Tuttle et al., 1973)

We now seek to determine the important parameters in the mixing process. For a fixed burner geometry the turbulent mixing time is inversely proportional to the turbulent root mean squared velocity. But the root mean squared velocity is a fraction of the mean convective velocity, so the mixing time is likewise inversely related to the mean convective velocity. For mixing controlled flames the pollutants should correlate with the inverse of a representative convective velocity.

Since CO results from flame quenching by fresh air, the representative velocity should be the air velocity through the liner air addition holes. For NO, the correlating velocity should be representative of the flow along the centerline with a heat addition effect.

In a combustor the distance a fluid particle travels affects the amount of time available for mixing; thus mixing times should be proportional to characteristic lengths of pollutant formation. For CO, the significant lengths tend to be associated with those to primary air addition holes and the related combustor diameters. For NO, the significant length is often related to the distance to the dilution holes and the corresponding diameter. These lengths match the regions of significant pollutant formation.

Combining these observations, we postulate a mixing time of the following form

$$\tau_{s\ell,em} = \ell_{em}/V_{em}$$

where $\tau_{s\ell,em}$: shear layer mixing time for a specific emission

$\ell_{em}$: characteristic length for the emission

$V_{em}$: characteristic velocity for the emission.

### C. Chemical Processes

After the fuel evaporates and mixes with the oxidizer, combustion can take place; here we will seek to characterize the chemical processes for CO and NO. CO is a combustion intermediate that exists in substantial concentrations within the recirculation zone and tends to burn out on the fresh air side of the shear layer. NO is a result of chemical combination of species in the air due to relatively high flame temperatures.

The reaction times are exponentially dependent on temperature. In Fig. 2-3, Sawyer et al. (1973) correlated $NO_x$ emissions from diffusion flame gas turbine engines as

$$\ln(NO_xEI/\text{constant}) = (-135\ \text{kcal/mole})/RT_{max}$$

where $NO_xEI$: emission index for nitric oxides

$R$: universal gas constant

$T_{max}$: calculated stoichiometric adiabatic flame temperature.

This temperature dependence coincides with that of the rate limiting step in thermal NO formation

$$O + N_2 \rightarrow NO + N$$

(assuming O atom equilibrium). Using this result, we define the chemical reaction time ($\tau_{no}$) for NO formation as

$$\tau_{no} = (\text{constant})\exp([135\ \text{kcal/mole}]/RT_{max})\text{msec}$$

Since a large percentage of the nitric oxides ($NO_x$) present are NO we assume that the above kinetic time is valid for all nitric oxides.

A CO reaction time is cast into a similar form. At a constant mixing time, burner CO emissions can be fitted to

$$\ln(COEI/\text{constant}) = E_{co}/RT_a$$

where COEI: emission index for carbon monoxide

$E_{co}$: activation energy for best data fit

$R$: universal gas constant

$T_a$: temperature characteristic of region of CO quenching.

Again, this implies that the reaction time for CO oxidation ($\tau_{co}$) can be expressed as an exponential;

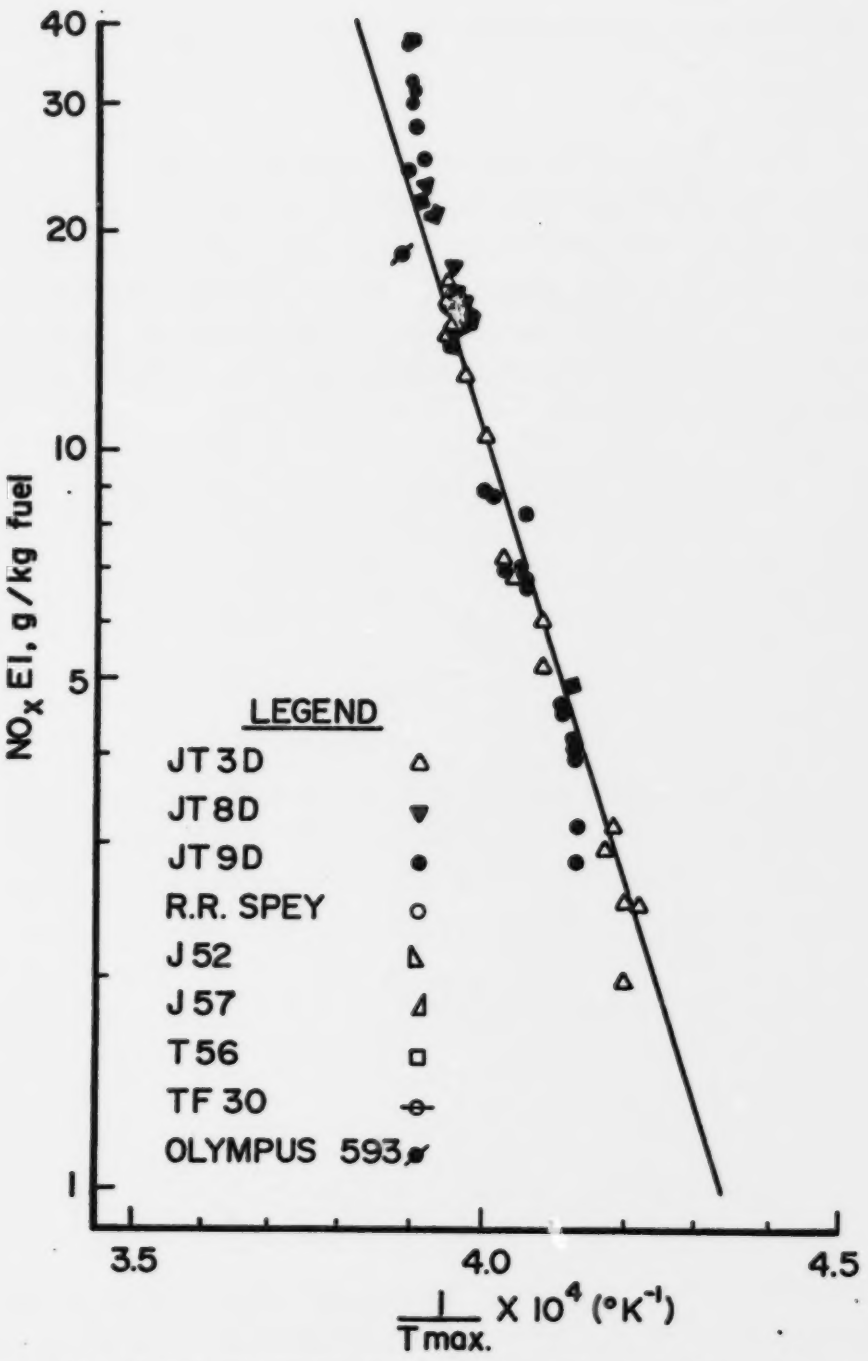


Figure 2-3. Correlation of $NO_x$EI with stoichiometric adiabatic flame temperature, based on combustor inlet air temperature (from Sawyer et al., 1973).

$$\tau_{co} = (\text{constant})\exp(E_{co}/RT_a)\text{msec.}$$

Now we have relationships characterizing the chemical processes for $NO_x$ and CO.

## D. Derivation of Characteristic Time Ratios

Having functions describing the dominant subprocesses of liquid fuel spray combustion, we now seek to find parameters composed of these functions capable of correlating pollutant emissions. In the following derivation (Tuttle et al., 1977), negligible heterogeneous effects will be assumed.

For the formation of NO (oxidation of CO) within a turbulent eddy of high temperature gas

$$d[NO]/dt \sim 1/\tau_{no}$$

and

$$d[CO]/dt \sim -[CO]/\tau_{co}$$

where brackets designate concentrations and t designates time. [O], $[N_2]$, and [OH] are assumed to be in excess. NO production (CO burnup) continues within fluid elements until the reaction rate is limited by mixing in of colder species. Integrating over the lifetime of the pollutant forming eddy

$$[NO] \sim \tau_{s\ell,no}/\tau_{no}$$

and

$$[CO]/[CO]_o \sim \exp(-A\tau_{s\ell,co}/\tau_{co}). \qquad 2\text{-}1$$

In the CO relationship $[CO]_o$ represents the concentration of CO in the recirculation zone (the source of CO for the shear layer) and A is an integration constant.

To relate the above expressions to the overall combustion process requires summing over all the reacting eddies of interest; however simplifications can be made. For $NO_x$, the number of eddies is expected to scale with the mass of fuel supplied; this implies

$$\Sigma [NO]/(\text{total mass of fuel}) \sim NO_x EI$$

where the summation is over all eddies of interest. Therefore,

$$NO_x EI \sim \tau_{s\ell,no}/\tau_{no}$$

A similar expression can be obtained for CO. The term $[CO]/[CO]_o$ represents the fraction of initial CO concentration remaining in a fluid element after time $\tau_{s\ell,co}$. $[CO]_o$ depends on the stoichiometry of the recirculation zone and thus the fuel flow rate. So,

$$[CO]/[CO]_o \sim COEI.$$

Looking at the right side of equation 2-1,

$$\exp(-A\tau_{s\ell,co}/\tau_{co}) \sim \tau_{co}/\tau_{s\ell,co}$$

for

$$-A\tau_{s\ell,co}/\tau_{co} >> 1.$$

Therefore

$$COEI \sim \tau_{co}/\tau_{s\ell,co}.$$

Droplet effects can be accounted for by perturbations on the parameters (Tuttle et al., 1976):

$$NO_x EI \sim \tau_{s\ell,no}/(\tau_{no} + K_1\tau_{eb})$$

and

$$COEI \sim (\tau_{co} + K_2\tau_{eb})/\tau_{s\ell,co}$$

$K_1$ and $K_2$ are constants. Notice that since $K_1$ and $K_2$ will be positive, heterogeneous effects tend to decrease $NO_x EI$ and increase COEI.

## E. Summary

For liquid fuel spray combustion in conventional gas turbine engines, $NO_x$ and CO can be correlated using the following expressions:

$$NO_x EI \sim \tau_{s\ell,no}/\tau_{no} \qquad 2\text{-}2$$

and

$$COEI \sim \tau_{co}/\tau_{s\ell,co}. \qquad 2\text{-}3$$

For the engines considered in this report droplet effects are assumed negligible; if droplet effects are considered the correlating expressions are

$$NO_x EI \sim \tau_{s\ell,no}/(\tau_{no} + K_1\tau_{eb})$$

and

$$COEI \sim (\tau_{co} + K_2\tau_{eb})/\tau_{s\ell,co}.$$

# III. CHARACTERISTIC TIME STUDIES ON THE GT-309 COMBUSTOR

The GT-309 is a regenerative, can-shaped , automotive gas turbine combustor designed by General Motors Corporation. In 1976, characteristic time parameters were used by Mellor (1977a) to correlate pollutant emissions for this burner; the data were obtained from the literature (Cornelius and Wade, 1970; Wade and Cornelius, 1972; Fredriksen, 1972) and General Motors personnel (Cornelius, 1976). A review of this work, plus a revised correlation for the GT-309, is presented in this section.

The GT-309 correlation has been revised because new definitions (as presented in this report) of the correlating parameters have been found to be more representative of gas turbine combustion phenomena, and because the validity of the original data is suspect. Currently the expression for the primary zone mass flow rate (Mellor, 1977b) is

$$\dot{m}_{a,\phi=1} = (fs)\dot{m}_{a,inlet}$$

where (fs) is the estimated fraction of the total flow through the primary zone; previously the expression was

$$\dot{m}_{a,\phi=1} = .8 \times .185\ \dot{m}_{a,inlet}.$$

Also, the reference area is now used for both the nitric oxides correlation and the carbon monoxide correlation; formerly the expression for carbon monoxide was

$$A_{hole} = \text{total area of air addition holes.}$$

Measurements at GMC (Hammond, 1977) indicate that the $NO_x$ levels used in the earlier analysis are probably incorrect. It is believed that the use of non-quenching, uncooled probes may have allowed continued NO

formation during sampling. Also, incomplete removal of water may have resulted in measurement errors; the water could produce positive interference with the NDIR analyzer and negative interference with the chemiluminescent analyzer.

Because of the above factors a new correlation is necessary.

## A. Sample Optimization

A purpose in the development of the characteristic time model is to provide the combustion engineer with a tool for designing low emissions burners. Traditionally, there has been assumed a trade-off between minimizing nitric oxides and minimizing carbon monoxide; for example, if the combustor temperatures were decreased nitric oxides went down and carbon monoxide went up, and vice versa. This section will show how the characteristic time model can be used to quantitatively predict the variation of emissions with combustor design and the results of such an optimization.

Using the early forms of the characteristic time definitions, Mellor correlated the nitric oxides for the GT-309 according to the following relation

$$NO_xEI = 0.865\ \tau_{s\ell,no}/\tau_{no} + 1.26 \qquad 3\text{-}1$$

and the carbon monoxide by

$$COEI = 0.947\ \tau_{co}/\tau_{s\ell,co} - 0.64. \qquad 3\text{-}2$$

Next, these correlations were used to predict how nitric oxides and carbon monoxide vary with changes in combustor geometry at two power points. The points chosen were the 90% setting and the 60% setting of the maximum gasifier speed; they represent a point where nitric oxides are the dominant pollutant present and a point where carbon monoxide is the dominant pollutant present, respectively.

Figures 3-1 and 3-2 (Mellor, 1977a) are graphical representations of the variations of emissions levels with combustor geometry; for two burner diameters, $NO_xEI$ and COEI are plotted versus the ratio of the length to air

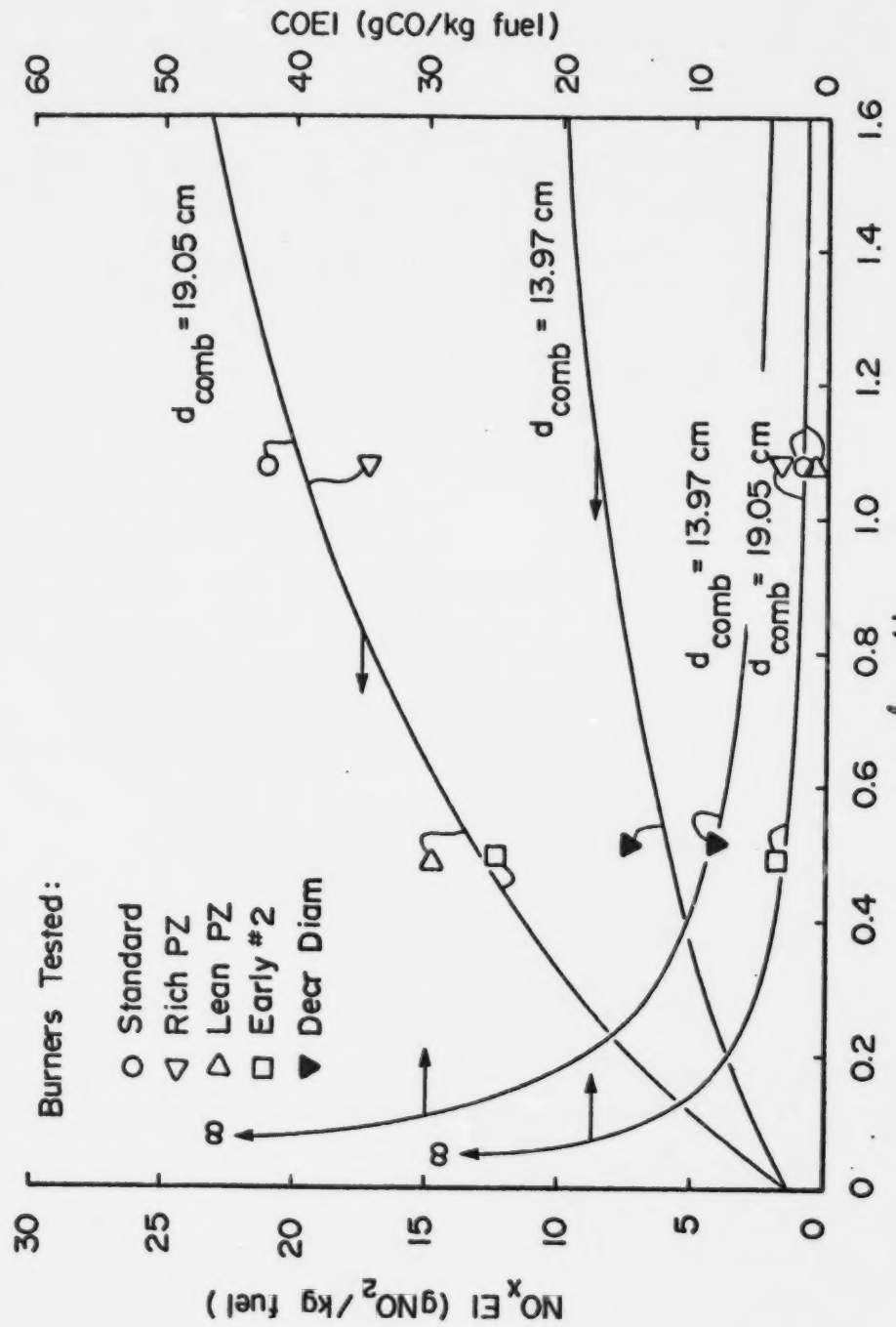


Figure 3-1. Variation of $NO_X$EI and COEI with combustor geometry at the 90% power point (from Tuttle et al., 1976)

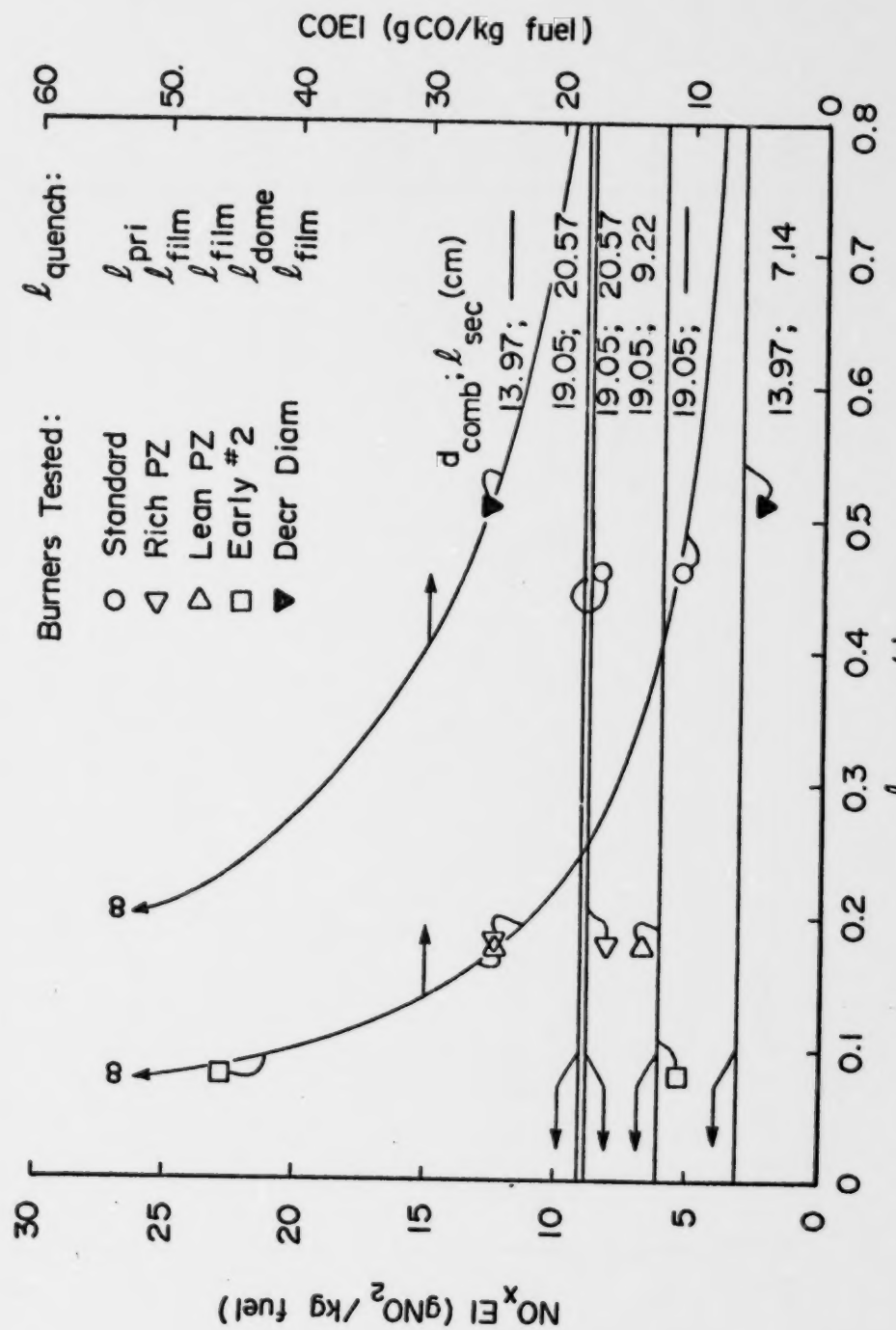


Figure 3-2. Variation of $NO_x$EI and COEI with combustor geometry at the 60% power point (from Tuttle et al., 1976).

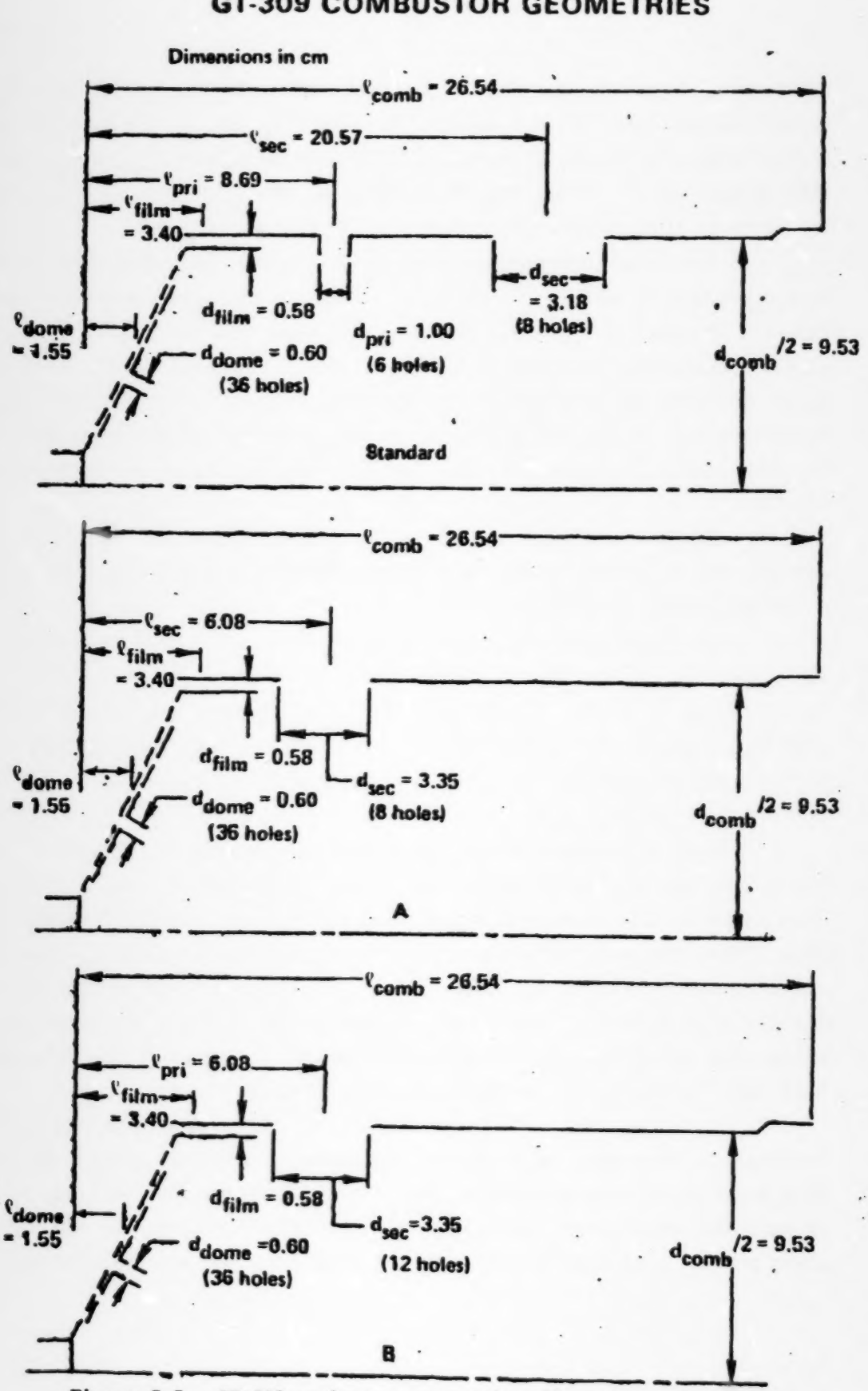


Figure 3-3. GT-309 combustor geometries (from Hammond, 1977).

addition holes and the diameter of the combustor. Measured points are also shown. Notice that Fig. 3-1 implies, for $0.6 < L_{sec}/d_{comb} < 1.6$, there is a relatively substantial decrease in $NO_x$EI with decreasing $L_{sec}/d_{comb}$, while COEI varies little. Also, Fig. 3-2 indicates, for $L_{quench}/d_{comb} > 0.6$, the variation in COEI is relatively small and $NO_x$EI is unaffected.

Using the information above, and retaining some successful features of the production burner, two emissions optimized combustors were designed. Fig. 3-3 (Hammond, 1977) shows the standard burner and the two modified versions. Notice that the primary holes have been eliminated and the secondary holes have been moved upstream; the number of secondary holes is the only difference between the two modified versions. The modified burners have the same diameter and the same dome and film cooling design as the standard burner.

The above recommendations were given to General Motors Corporation who then built and tested the standard and modified burners (Hammond, 1977). A review of this work follows.

For comparison, the run conditions of Cornelius and Wade were duplicated for all burners. This included, in terms of gasifier shaft speed, points at 50, 60, 70, 80, 90 and 100% of the maximum. It was found that the standard burner was stable at all points tested, that modified burner A was unstable at 50 and 60%, and that modified burner B was unstable at 50% and marginally stable at 60%.

Fig. 3-4 summarizes the results of the testing for nitric oxides. Notice that for all points except the 90 and 100% levels for the standard burner, the correlations fall within one standard deviation of the measured data. Also, the modified burners show reductions in nitric oxides from the standard where the $NO_x$EI for combustion A is 47 to 49% lower and the $NO_x$EI for combustor B is 37 to 61% lower. In all of these cases, the predicted values were corrected for the estimated measurement errors in the original data; care was taken not to duplicate the errors for the new data.

Likewise, Fig. 3-5 summarizes the results of the carbon monoxide testing. In this case, most of the predictions do not fall within one standard deviation of the measured values. Specifically, combustor A was predicted to emit 215% more carbon monoxide than the standard combustor at the highest power point. Actually, for the range of speeds tested, measurements indicate

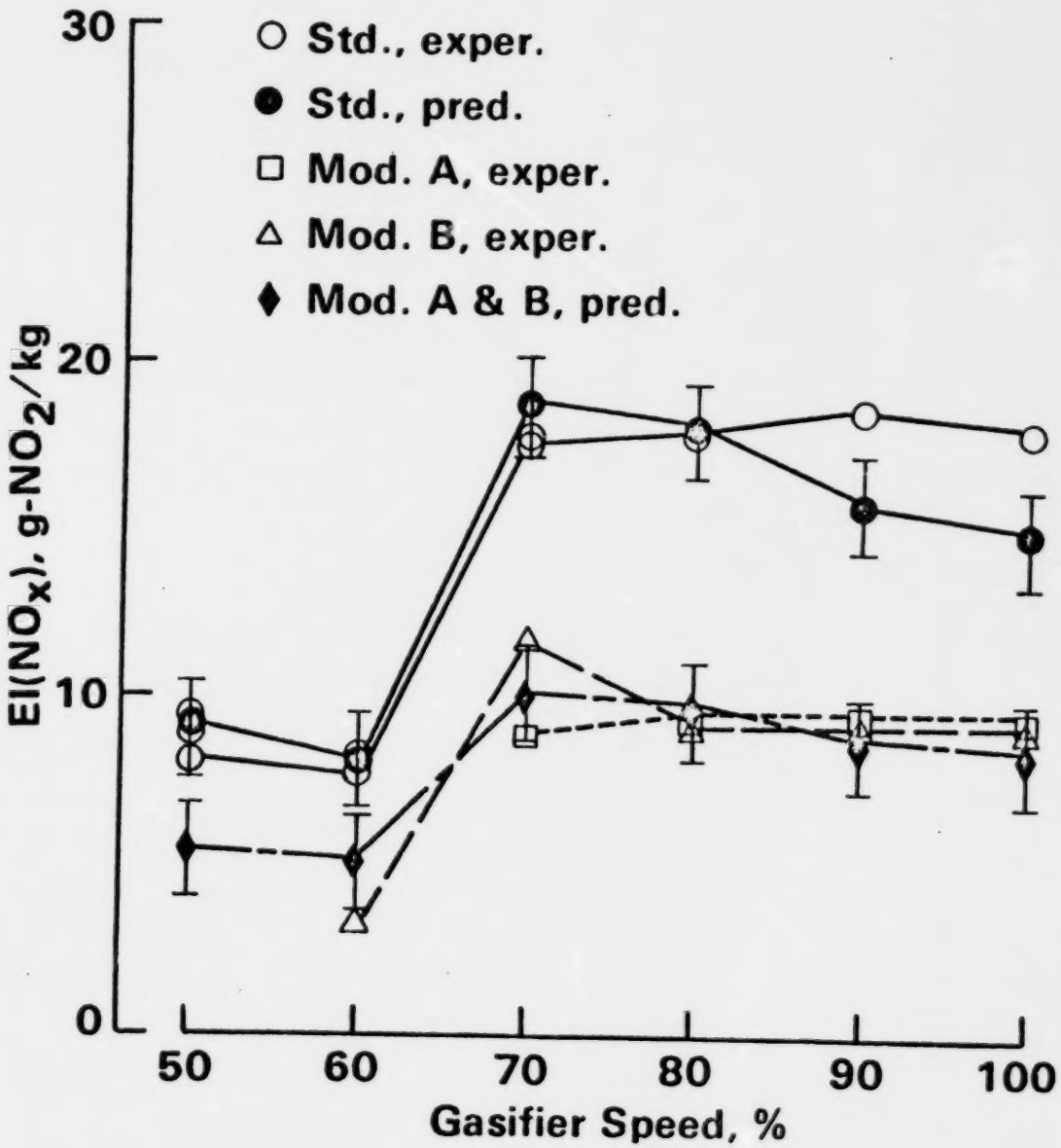


Figure 3-4. Comparison of predicted and experimental EI($NO_x$) versus gasifier speed (from Hammond, 1977).

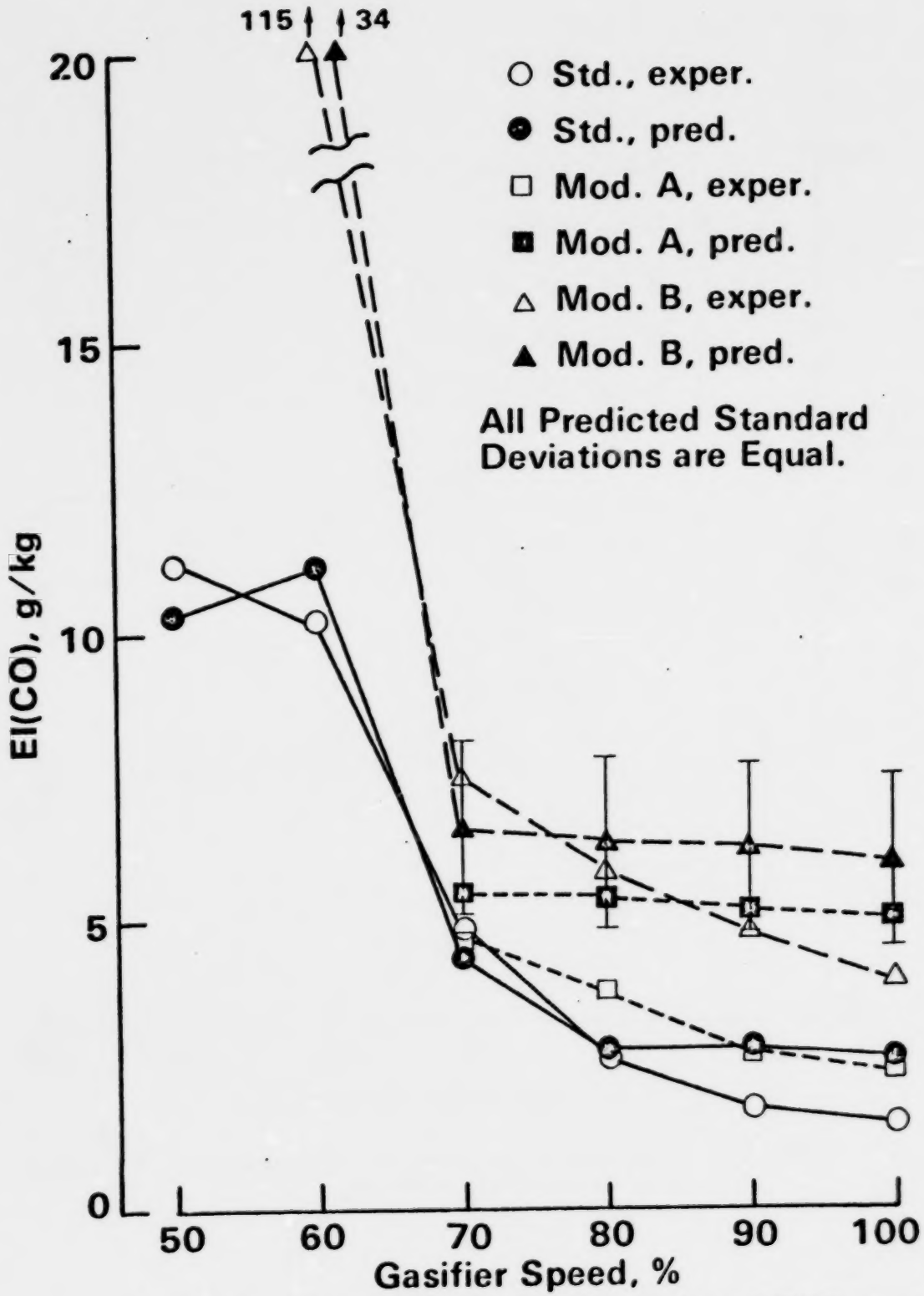


Figure 3-5. Comparison of predicted and experimental EI(CO) versus gasifier speed (from Hammond, 1977).

the increase was from 6 to 59%. It was predicted that combustor B would produce 32% less carbon monoxide than combustor A, but the emission levels for combustor B were actually from 55 to 81% higher.

In summary, the model's predictions for nitric oxides show close agreement with measurements, but problems still exist with predicting carbon monoxide. However, it is encouraging that combustor A produced substantially less nitric oxides than the standard burner with only marginal increases (below predictions) in carbon monoxide.

### B. Current GT-309 Correlation

Because previous GT-309 characteristic time correlations had used obsolete parameter definitions and suspect data (Hammond, 1977) a new correlation is necessary; this time, of course, the current parameter definitions and reliable data are used. The data are from the GMC optimization test for the burners shown in Fig. 3-3. A computer program is used for the analysis.

For the nitric oxides correlation the definitions and terms below are used. These are

$$\tau_{no} = 10^{-12}\exp(135/RT_{\phi=1}) \qquad 3\text{-}3$$

$$\tau_{s\ell,no} = \ell_{no}/V_{\phi=1} \qquad 3\text{-}4$$

$$\ell_{no}^{-1} = \ell_{quench}^{-1} + d_{comb}^{-1} \qquad 3\text{-}5$$

$$V_{\phi=1} = (fs)\dot{m}_a RT_{\phi=1}/PM\frac{\pi}{4}d^2_{comb}. \qquad 3\text{-}6$$

The first definition is for the chemical kinetic time for the formation of nitric oxide. Inside the exponential, the numerator is the activation energy of nitric oxide formation in kilocalories per gram-mole. Also, the R stands for the universal gas constant and the $T_{\phi=1}$ stands for the calculated stoichiometric flame temperature.

The second definition is for the shear layer mixing time. As explained in Section II, this is taken as the ratio of a length and a velocity characteristic of the region of a pollutant's formation. In the third defini-

tion, the characteristic length is computed as the reciprocal sum of reciprocals; the quench length, for all GT-309 power points, is assumed to be $\ell_{sec}$ shown in the figures in Fig. 3-3. In the fourth definition, the terms composing the stoichiometric flame zone velocity are

(fs): estimated fraction of mass flow through the primary zone

P: burner static pressure

M: molecular mass of air;

the rest of the terms are as explained earlier.

Fig. 3-6 shows the correlation for nitric oxides, with $NO_xEI$ plotted versus $\tau_{s\ell,no}/\tau_{no}$. The equation of the fit is

$$NO_xEI = 2.583\ \tau_{s\ell,no}/\tau_{no} + 1.104; \qquad 3\text{-}7$$

the correlation coefficient (r) is equal to .8992. For reference, a correlation coefficient of 1.0 is a perfect correlation, of 0.0 is no correlation, and of 0.9 (or higher) is generally considered a good correlation.

(fs) for the above correlation is calculated as the fraction of the total air addition hole area upstream of the assumed quench location, but part of the flow entering the primary zone through the holes at the quench length goes upstream (Roberts et al., 1971). An estimate of the fraction of the flow through an individual hole going upstream is

$$k = 0.5[T_{in}/T_{pz}]^{1/2} \cos \beta_o \qquad 3\text{-}8$$

where

k: fraction of the flow going upstream

$T_{in}$: inlet temperature

$T_{pz}$: primary zone temperature

$\beta_o$: angle (measured from a radial cross-section) at which the flow enters the primary zone.

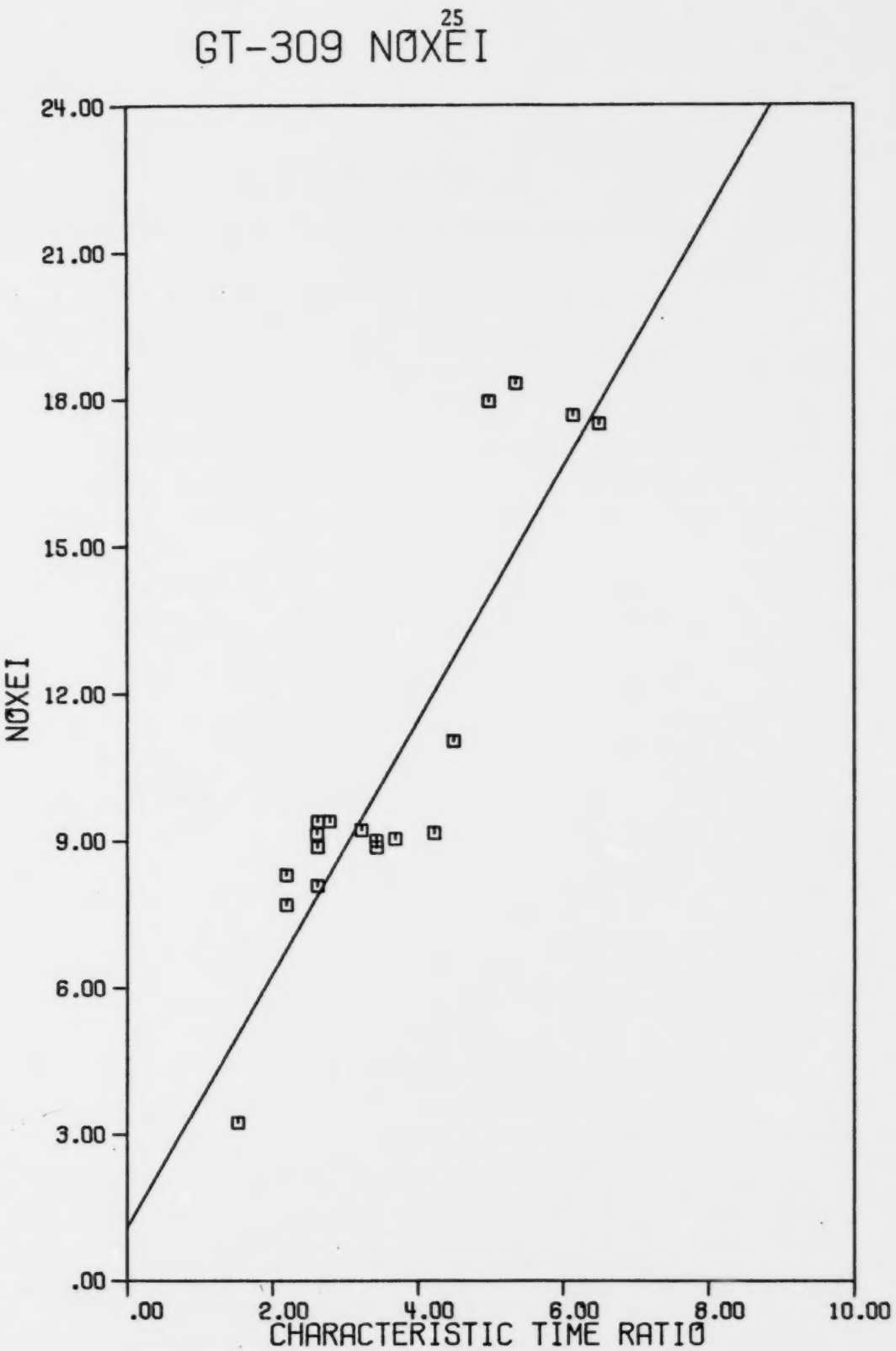


Figure 3-6. Correlation of the GT-309 $NO_x$EI data.

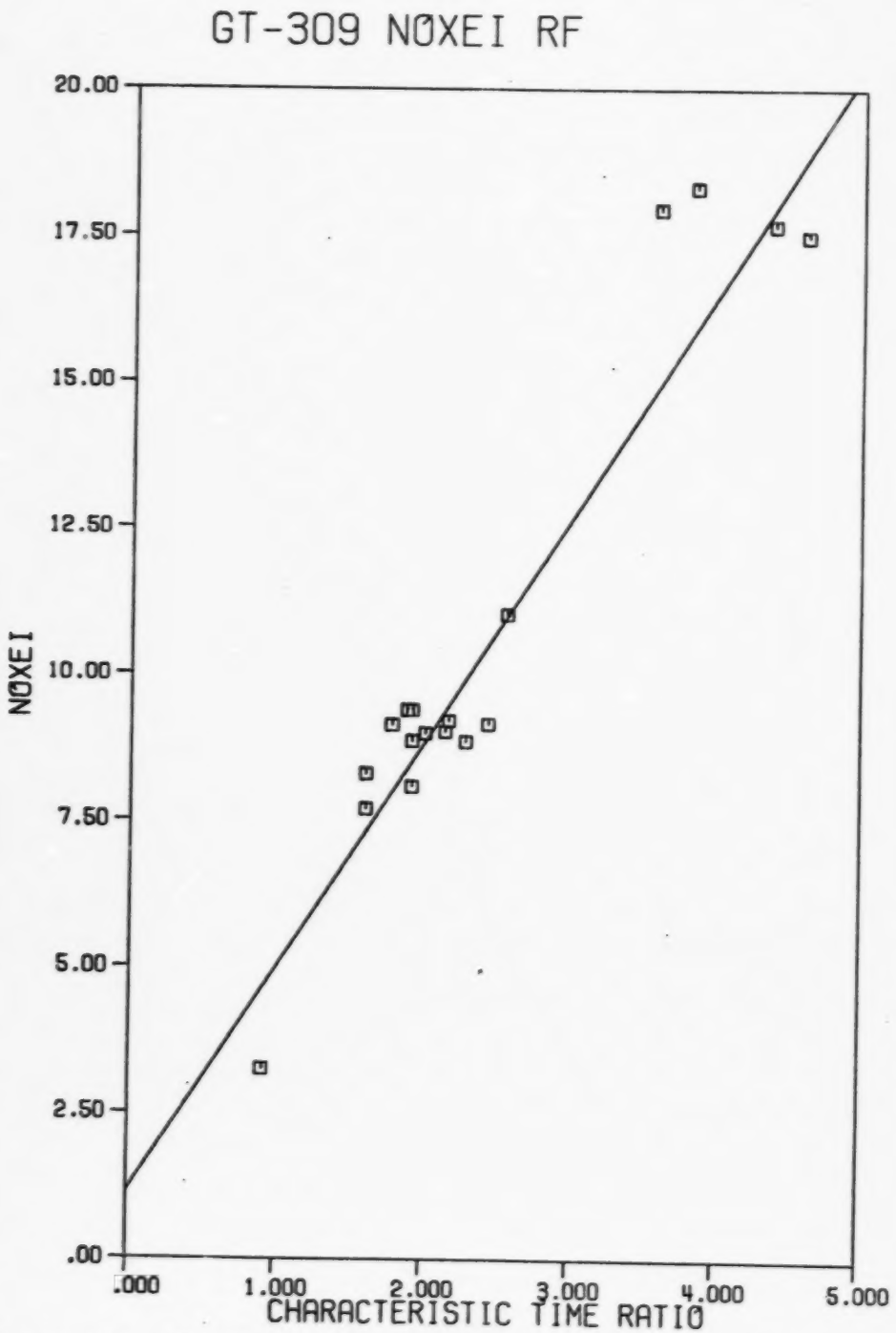


Figure 3-7. Correlation of the GT-309 $NO_x$EI data assuming reversing flow.

Assuming the primary zone temperature is equal to the stoichiometric flame temperature and the flow through the air addition holes enters perpendicularly to the flow in the combustor an alternate correlation was done. The result (shown in Fig. 3-7) is

$$NO_x EI = 3.836\ \tau_{s\ell,no}/\tau_{no} + 1.161 \qquad 3\text{-}9$$

with r equal to .9548.

The definitions used in the carbon monoxide correlation are of the same form as those used in the nitric oxides correlation. They are

$$\tau_{co} = 10^{-3}\exp(10.76/RT_{avg}) \qquad 3\text{-}10$$

$$T_{avg} = (T_{in} + T_{out})/2 \qquad 3\text{-}11$$

$$\tau_{s\ell,co} = \ell_{co}/V_{ref} \qquad 3\text{-}12$$

$$\ell_{co}^{-1} = \ell_{quench}^{-1} + d_{comb}^{-1} \qquad 3\text{-}13$$

$$V_{ref} = \dot{m}_a RT_{in}/PM\frac{\pi}{4} d^2_{comb}. \qquad 3\text{-}14$$

In the first definition $\tau_{co}$ is the chemical kinetic time for the oxidation of carbon monoxide, 10.76 is the activation energy for carbon monoxide in kilocalories per gram-mole, R is (again) the universal gas constant, and $T_{avg}$ (as shown in equation 3-11) is the average of the inlet and the outlet temperatures.

The third and fourth definitions are analogous to the second and third ones, respectively, used for nitric oxides. However, in this case, the quench length is allowed to vary between the length to the film cooling slot, to the primary holes (when they are present), to the secondary holes, and the differences between these lengths; the computer program mentioned before is used to determine the best correlation using combinations of these lengths.

The reference velocity is expressed by the last definition. Notice that it is defined the same way as the stoichiometric velocity except there

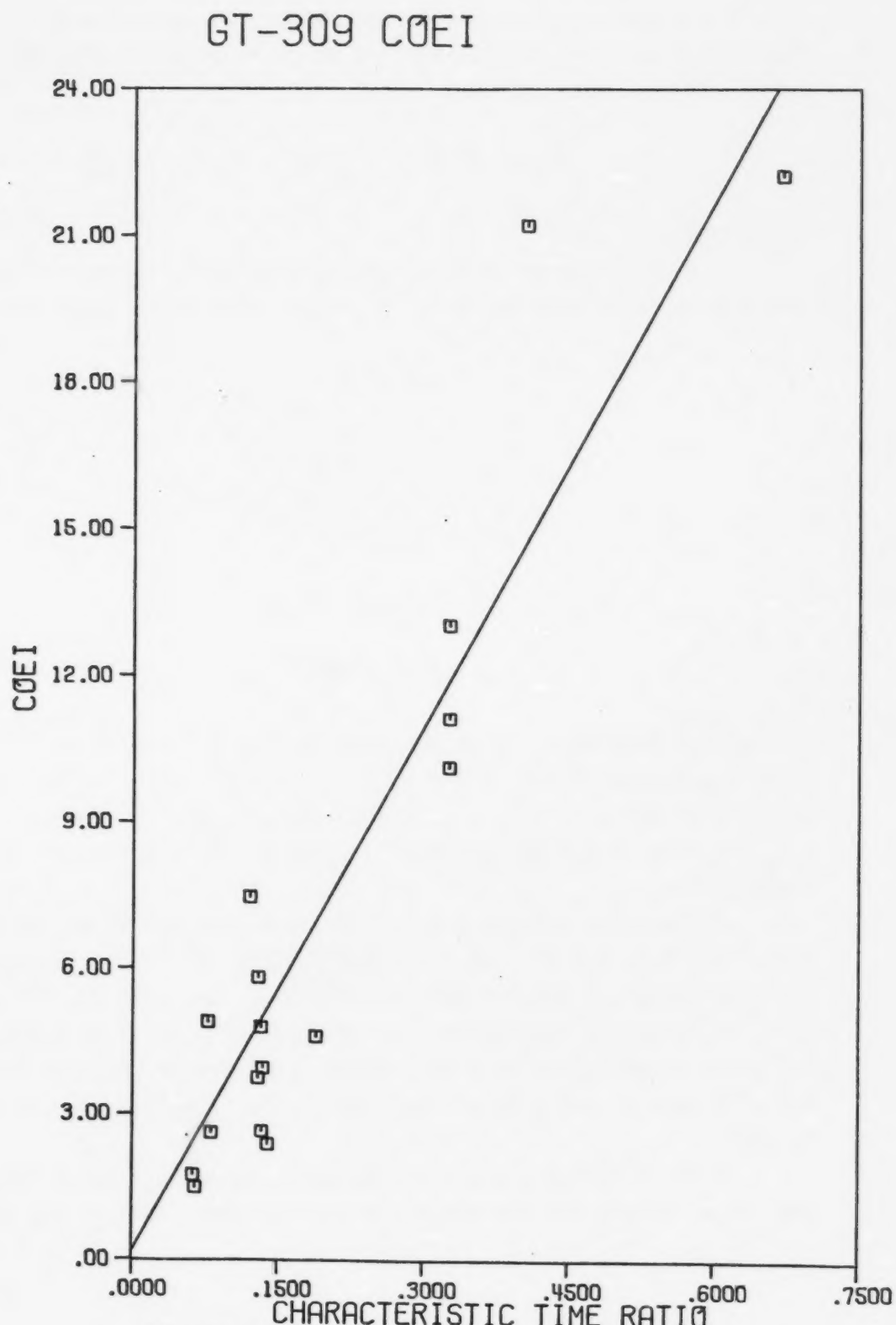


Figure 3-8. Correlation of the GT-309 COEI data.

is no flow splitting assumed and the inlet temperature is used instead of the stoichiometric flame temperature.

Fig. 3-8 shows the correlation for carbon monoxide, with COEI plotted versus $\tau_{co}/\tau_{s\ell,co}$. The equation of the fit is

$$COEI = 35.493\ \tau_{co}/\tau_{s\ell,co} + 0.739, \qquad 3\text{-}15$$

and the correlation coefficient is .9440. Table 3-1 summarizes the $\ell_{quench}$'s chosen for the correlation.

Table 3-1. Quench Length for the GT-309 Carbon Monoxide Correlation

| Power | Std. | Mod A | Mod B |
|---|---|---|---|
| 50 | film or pri | ----- | ----- |
| 60 | sec-pri | ----- | ----- |
| 70 | sec-pri or pri | film | sec |
| 80 | sec-pri | sec | sec |
| 90 | sec | sec | sec |
| 100 | sec | sec | sec |

where

film: film cooling slot

pri: primary air addition holes

sec: secondary dilution holes.

In summary, the characteristic time model correlates the new nitric oxide data and the carbon monoxide data for the GT-309 quite well.

## C. Summary

The use of the characteristic time model for designing optimum (with respect to emissions) combustors is demonstrated for the GT-309 burner. The designed burners, built and tested by General Motors Corporation, show good agreement with nitric oxides predictions, but show significant deviations

from the carbon monoxide predictions.

Correlations for the new data obtained for the GT-309 are below. The correlations for nitric oxides neglecting reverse flow and accounting for reverse flow follow, respectively,

$$NO_xEI = 2.583\ \tau_{s\ell,no}/\tau_{no} + 1.104 \qquad 3\text{-}7$$

$$NO_xEI = 3.836\ \tau_{s\ell,no}/\tau_{no} + 1.161. \qquad 3\text{-}9$$

The correlation for carbon monoxide is

$$COEI = 35.493\ \tau_{co}/\tau_{s\ell,co} + 0.793. \qquad 3\text{-}15$$

# IV. CHARACTERISTIC TIME STUDIES ON THE T-63 COMBUSTOR

In the present section we consider several applications of the model to a second gas turbine combustor, the Detroit Diesel Allison T-63 helicopter liner. Considerable data are available for this burner showing the effects of both geometry and fuel injector variation (Troth et al., 1973, 1974) and fuel type variation (Moses, 1975) upon pollutant emissions. The geometries tested include several advanced combustors of the prevaporizing/premixing type and some utilizing film fuel injection; in addition the heavier fuels tested show evidence of heterogeneous effects as well as those due to nitrogen bound in the fuel (#5 oil). Also, unburned hydrocarbon emissions data are available for the T-63 to yield a hydrocarbons emissions index correlation.

The correlating parameters for negligible heterogeneous effects are the same as those used for the GT-309 correlation:

$$NO_x EI \sim \tau_{s\ell,no}/\tau_{no} \qquad 4\text{-}1$$

$$COEI \sim \tau_{co}/\tau_{s\ell,co} \qquad 4\text{-}2$$

Again, the chemical kinetic times for nitric oxidation formation and carbon monoxide oxidation are

$$\tau_{no} = 10^{-12}\exp(135/RT_{\phi=1}) \qquad 4\text{-}3$$

$$\tau_{co} = 10^{-3}\exp(10.76/RT_{avg}) \qquad 4\text{-}4$$

It should be noted that in Eq. 4-3 $T_{\phi=1}$ (the adiabatic stoichiometric flame temperature) is a function of fuel type, inlet air temperature, and pressure.

Table 4-1. T-63 Combustor Operating Conditions (Troth et al., 1973) and Computed Chemical Kinetic Times (JP4 Fuel)

| % of Design Speed | Inlet Air Temperature, °K | Inlet Pressure, atm | Air Flow Rate, kg/sec | Fuel Flow Rate, kg/hr | Burner Outlet Temperature, °K | Computed $T_{\phi=1}$, °K[a] | $\tau_{no}$, msec[a] | $\tau_{co}$, msec[a] |
|---|---|---|---|---|---|---|---|---|
| A. Non-Regenerative Cycle | | | | | | | | |
| 10 | 422 | 3.03 | .849 | 33.46 | 834 | 2364 | 3.03 | 5.58 |
| 40 | 476 | 4.34 | 1.149 | 54.03 | 972 | 2398 | 2.02 | 1.78 |
| 55 | 494 | 4.87 | 1.249 | 65.15 | 1032 | 2409 | 1.77 | 1.21 |
| 75 | 518 | 5.52 | 1.353 | 81.04 | 1121 | 2423 | 1.51 | .740 |
| 100 | 547 | 6.28 | 1.462 | 104.19 | 1244 | 2439 | 1.25 | .423 |
| B. Regenerative Cycle | | | | | | | | |
| 10 | 626 | 2.93 | .799 | 23.15 | 932 | 2449 | 1.12 | 1.05 |
| 40 | 653 | 4.10 | 1.117 | 37.68 | 1008 | 2472 | .864 | .678 |
| 55 | 681 | 4.46 | 1.190 | 45.85 | 1078 | 2486 | .740 | .472 |
| 75 | 722 | 5.12 | 1.276 | 55.39 | 1161 | 2508 | .582 | .315 |
| 100 | 794 | 5.80 | 1.380 | 69.92 | 1307 | 2543 | .401 | .173 |

[a]See text for definition.

Table 4-2. T-63 Combustor Operating Conditions (Moses, 1975) and Computed Chemical Kinetic Times

| | | | | | JP4 Fuel | | | |
|---|---|---|---|---|---|---|---|---|
| % of Design Speed | Inlet Air Temperature, °K | Inlet Pressure, atm | Air Flow Rate, kg/sec | Fuel Flow Rate, kg/hr | Burner Outlet Temperature, °K | Computed $T_{\phi=1}$, °K[a] | $\tau_{no}$, msec[a] | $\tau_{co}$, msec[a] |
| 10 | 422 | 2.49 | .699 | 27.6 | 856 | 2359 | 3.22 | 4.81 |
| 25 | 451 | 3.07 | .821 | 35.4 | ---- | 2377 | 2.59 | ---- |
| 40 | 477 | 3.58 | .948 | 44.4 | 978 | 2393 | 2.14 | 1.71 |
| 55 | 494 | 4.12 | 1.030 | 53.4 | 1043 | 2404 | 1.88 | 1.15 |
| 75 | 517 | 4.55 | 1.120 | 66.6 | 1136 | 2417 | 1.61 | .700 |
| 100 | 546 | 5.18 | 1.210 | 85.8 | 1265 | 2433 | 1.34 | .396 |

| Jet A Fuel | | | | Diesel Fuel 2 | | | | #5 Oil | | | |
|---|---|---|---|---|---|---|---|---|---|---|---|
| Burner Outlet Temperature, °K | Computed $T_{\phi=1}$, °K[a] | $\tau_{no}$, msec[a] | $\tau_{co}$, msec[a] | Burner Outlet Temperature, °K | Computed $T_{\phi=1}$, °K[a] | $\tau_{no}$, msec[a] | $\tau_{co}$, msec[a] | Burner Outlet Temperature, °K | Computed $T_{\phi=1}$, °K[a] | $\tau_{no}$, msec[a] | $\tau_{co}$, msec[a] |
| 856 | 2351 | 3.55 | 4.81 | 846 | 2341 | 4.02 | 5.14 | 839 | 2333 | 4.44 | 5.36 |
| ---- | 2369 | 2.85 | ---- | 909 | 2360 | 3.18 | 2.86 | 901 | 2352 | 3.51 | 3.03 |
| 978 | 2385 | 2.35 | 1.71 | 967 | 2375 | 2.65 | 1.82 | 959 | 2367 | 2.92 | 1.89 |
| 1043 | 2396 | 2.07 | 1.15 | 1032 | 2387 | 2.30 | 1.21 | 1023 | 2379 | 2.53 | 1.26 |
| 1136 | 2409 | 1.77 | .700 | 1123 | 2400 | 1.97 | .740 | 1113 | 2392 | 2.17 | .771 |
| 1265 | 2426 | 1.45 | .396 | 1250 | 2416 | 1.63 | .417 | 1239 | 2408 | 1.79 | .431 |

[a]See text for definition.

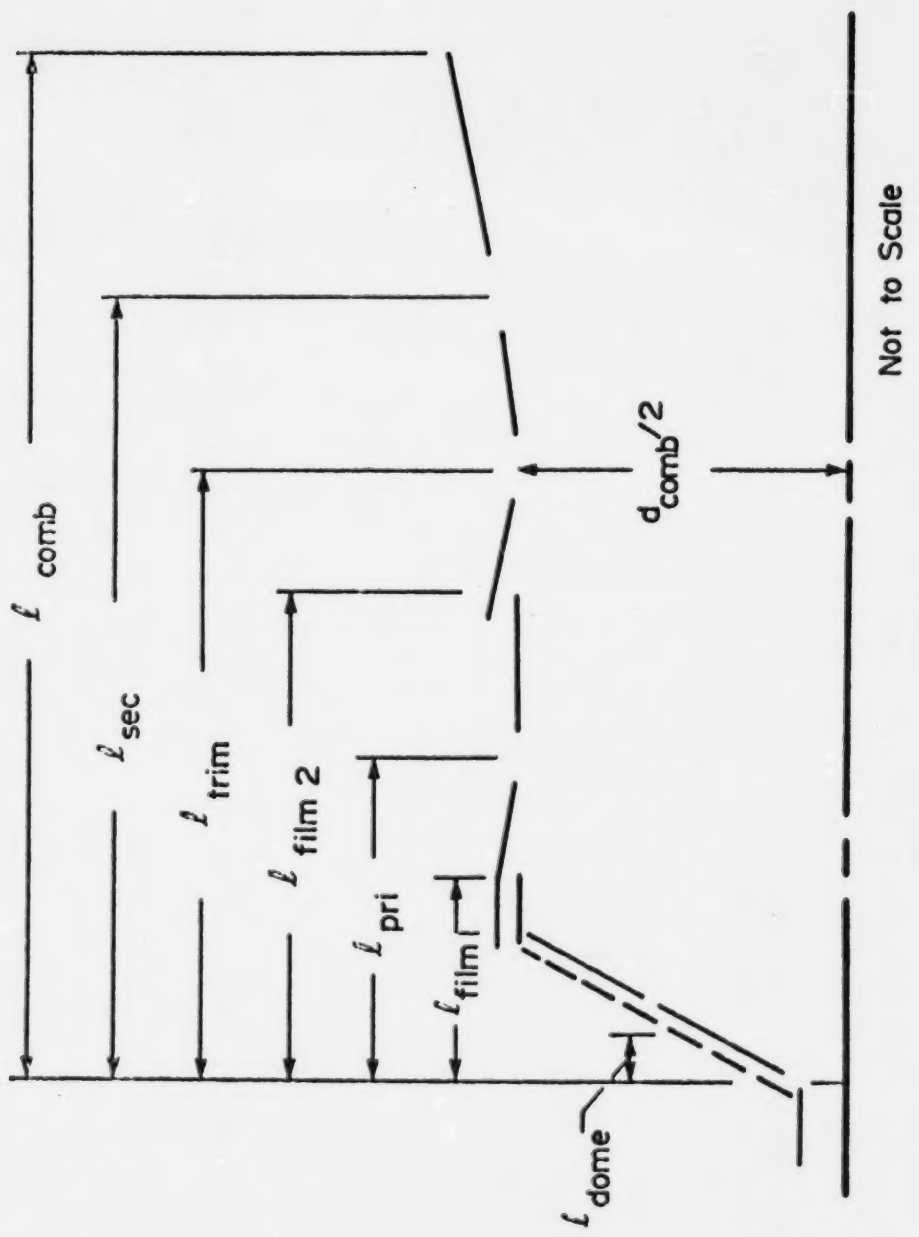


Figure 4-1. The T-63 baseline burner geometry.

The T-63 non-regenerative and regenerative combustor inlet concitions are given in Table 4-1 (Troth et al., 1973). $T_{\phi=1}$ were calculated for JP 4 fuel, $T_{avg}$ from burner outlet temperatures listed by Troth et al. (1973), and $\tau_{no}$ and $\tau_{co}$ from Eq. 4-3 and 4-4 above. Moses (1975) used somewhat different non-regenerative inlet conditions and the additional fuels Jet A, DF 2, and #5 oil: these are listed in Table 4-2, along with computed temperatures and kinetic times. Troth et al. (1973, 1974) tested over nineteen different combustor geometries, including conventional, film fuel injected, and prevaporizing/premixing burners. Some of the designs are radically different from the baseline (Fig. 4-1), and the interested reader is referred to their 1973 report for the details of the geometry as well as the pollutant emissions of HC, CO, and $NO_x$. In that report details of four different hollow spray cone fuel injectors used with the baseline burner may also be found. Their nomenclature will be preserved here for convenience.

Moses (1975) results were all obtained with the baseline burner and dual/orifice pressure atomizing fuel injector. Only HC, CO and NO emissions were reported; the $NO_2$ values listed in Table 4-3 were provided via personal communication.

Table 4-3. T-63 $NO_2$ Emissions
(Moses, 1976)

| | $NO_2$, ppm | | | |
|---|---|---|---|---|
| % of Design Speed | JP 4 | Jet A | DF 2 | #5 Oil |
| 10 | 10.0 | 17.0 | 1.8 | 0 |
| 25 | 9.7 | 15.7 | 0.8 | - |
| 40 | 8.4 | 14.3 | 0.9 | - |
| 55 | 7.8 | 13.0 | 0 | 0 |
| 75 | 6.0 | 10.3 | 0 | - |
| 100 | 3.0 | 9.0 | 0 | 0 |

### A. $NO_x$EI Correlation

The best $NO_x$EI correlation for the GT-309 combustor was found to be of the form

$$NO_x EI \sim \tau_{s\ell,no}/\tau_{no} \qquad 4\text{-}1$$

where

$$\tau_{s\ell,no} = \ell_{no}/V_{\phi=1} \qquad 4\text{-}5$$

$$V_{\phi=1} \sim \dot{m}_a RT_{\phi=1}/PM\frac{\pi}{4}d_{comb}^2 \qquad 4\text{-}6$$

Again, $\ell_{no}$ is the macroscale for NO formation (a function of combustor geometry) and $V_{\phi=1}$ is an estimate of the velocity with which stoichiometric eddies flow down the liner. $\dot{m}_a$ is the total air flow rate, P is combustor pressure, M is molecular weight (taken as that of air for convenience), and $d_{comb}$ is the burner diameter at the axial location of the quench position.

Thus changes in inlet conditions and fuel type with fixed geometry (fixed $\ell_{no}$ and dome) should be correlated by the appropriate changes in $\tau_{no}$ and $V_{\phi=1}$. Mellor (1977b) performed such a correlation for the standard burner and deduced that it was valid. In addition, the results indicate that heterogeneous effects are negligible, so now data for various injectors can be included. As with the GT-309, data from different geometries can be correlated. The correlation (shown in Fig. 4-2) below includes all of the data mentioned above:

$$NO_x EI = 6.882\ \tau_{s\ell,no}/\tau_{no} + 0.686 \qquad 4\text{-}7$$

with r = .9223. $V_{\phi=1}$ for the T-63 standard combustor has been defined as

$$V_{\phi=1} = .606\dot{m}_a RT_{\phi=1}/PM\frac{\pi}{4}d^2 \qquad 4\text{-}8$$

where $(.606m_a)$ is an estimate of the primary zone air flow split based on the percentage of air-addition area upstream of the assumed quench location. See Table 4-4 for a listing of the observed NO quench lengths, which correspond to the axial location of the trim holes (see Fig. 4-1).

As noted in Mellor (1977b), correlations of these data show that $NO_x EI$ is independent of fuel and injector type. Thus droplet effects can

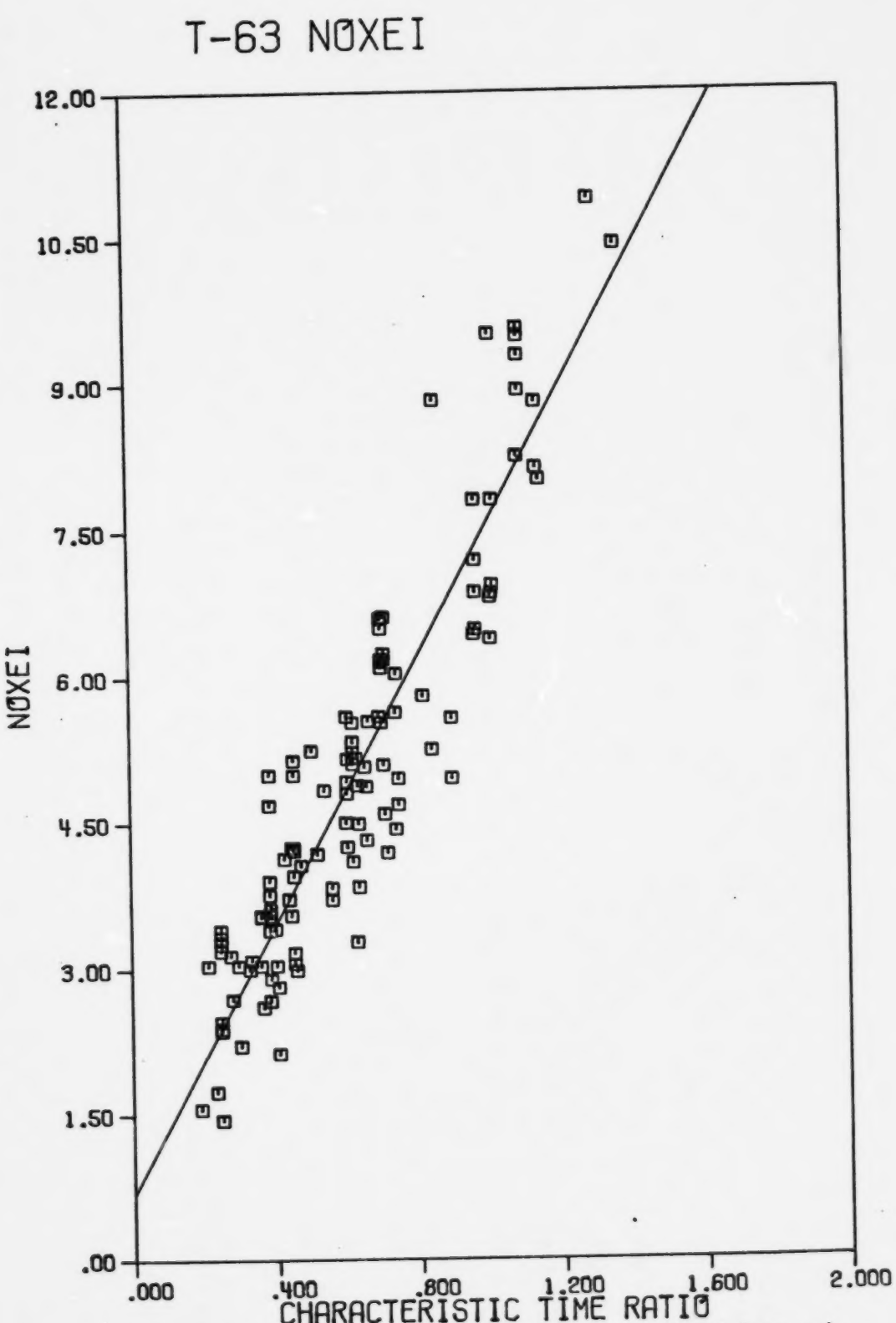


Figure 4-2. Correlation of the T-63 (conventional burners) COEI data.

Table 4-4. Macroscales for
T-63 NO And CO Emissions

| Burner[a] | $\ell_{no}$, cm | $\ell_{co}$, cm | Burner[a] | $\ell_{no}$, cm | $\ell_{co}$, cm |
|---|---|---|---|---|---|
| Standard | 5.69 | 2.99(T) | Var Geom 0% Open | 4.07 | 4.11(P)[c], 2.77(FI)[d], 1.35(D)[e] |
| Extended Length | 8.88 | 8.02(T) | Annular Dilution | 8.24 | 6.74(T) |
| EQ & Ext Length | 8.88 | 8.28(T), 3.23(P)[b] | Canted Primary | 9.40 | 8.64(T)[c,d], 4.11(P)[f], 2.77(FI)[b,g] |
| Delayed Dilution | 8.24 | 6.52(T) | Canted Mod A | 9.40 | 8.64(T) |
| Ext Length & DQ | 8.83 | 7.39(T) | Swirl Dome, Film | 10.23 | 8.23(T) |
| Opt Prim | 8.88 | 8.01(T) | Rich Premix, Swirl | 10.54 | 8.50(T) |
| Pepper Pot | 8.88 | 8.88(T) | Premix/Prevap | 10.42 | 9.12(T) |
| Rich PZ | 5.69 | 4.68(S) | Prech, Film | 9.34 | 5.70(T) |
| Var Geom 20% Open | 9.60 | 8.71(T) | Prech, P Atom | 9.34 | 5.70(T) |

[a] See Troth et al. (1973) for configuration.

[b] 40% point.

[c] 100% point.

[d] 75% point.

[e] 55 and 40%.

[f] 55% point.

[g] 10% point.

S = secondary holes, T = trim holes, P = primary holes,
Fl = first film cooling slot, D = dome holes.

be safely ignored, and the predominant effect of fuel type on $NO_x$EI is contained in $T_{\phi=1}$. An exception to this is #5 oil data where this fuel's (and only this fuel's) substantial nitrogen content (Moses, 1975) results in higher than normal $NO_x$EI. The collapse of the data (within the scatter) also indicates that geometry effects are correctly accounted for.

B. COEI Correlation

As for the GT-309 COEI correlation, the mean of the inlet air and the burner outlet temperatures was used in the kinetic time (Eq. 4-4) for the T-63. After an initial correlation of the T-63 Mellor (1977b) notes that data points for Diesel fuel and #5 oil fail to correlate well with the data for JP 4 and Jet A. This is attributed to non-negligible droplet lifetimes for these fuels and the specific atomizers used; Mellor then recommends that the following expression be used for the correlation

$$COEI \sim (\tau_{co} + K\tau_{eb})/\tau_{s\ell,co} \qquad 4\text{-}9$$

where $\tau_{eb}$ is the droplet evaporation time and K is chosen to maximize r. This new correlation has not been performed yet because of limited experience in estimating the requisite transfer numbers, etc., for multicomponent fuels.

For the T-63 combustor $\tau_{s\ell,co}$ is defined as

$$\tau_{s\ell,co} = \ell_{co}/V_{ref} \qquad 4\text{-}10$$

where

$$\ell_{co}^{-1} = \ell_{quench}^{-1} + d_{comb}^{-1} \qquad 4\text{-}11$$

with the $\ell_{quench}$, or $\ell_{quench's}$, for each burner designated in Table 4-4. A shift in $\ell_{quench}$ with power level seems restricted to combustors with a substantial fraction of the air through the primary zone. For cases where the shift occurs $\ell_{quench}$ is taken as the appropriate axial length to the air addition point.

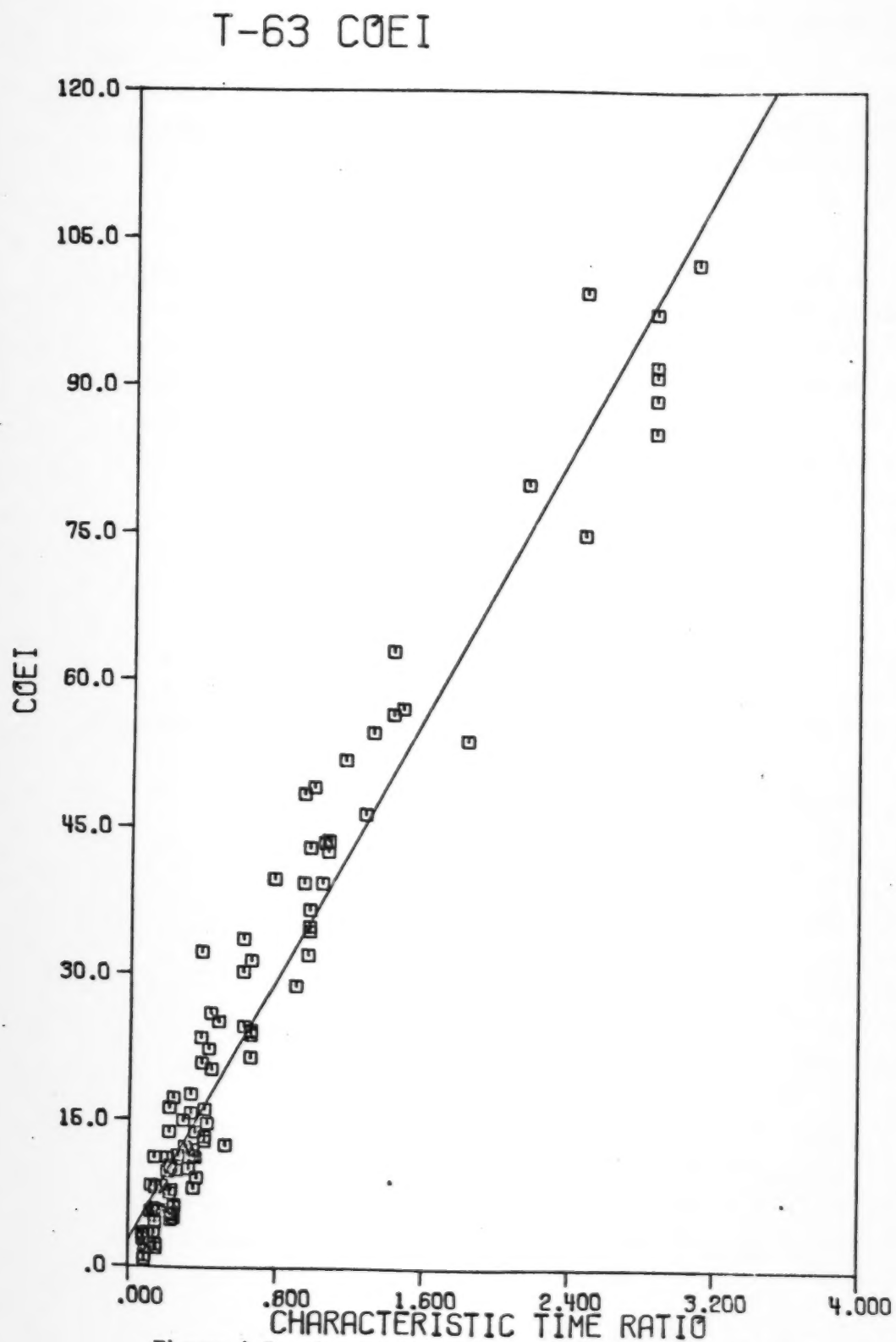


Figure 4-3. Correlation of the T-63 (conventional burners) COEI data.

For the other T-63 combustors labelled T and S in Table 4-4 the best correlation was obtained with $\ell_{quench}$ defined as the axial distance from the primary air holes to the trim (T) or secondary (S) holes, so that

$$\ell_{co}^{-1} = (\ell_{trim\ or\ sec} - \ell_{pri})^{-1} + d_{comb}^{-1} \qquad 4\text{-}12$$

COEI for the T-63 liner was correlated with reference velocity:

$$V_{ref} = \dot{m}_a RT_{in}/PM\frac{\pi}{4}d_{ref}^2 \qquad 4\text{-}13$$

where $d_{ref}$ was taken as 16.64 cm (Troth et al., 1973). The resulting correlation (given in Fig. 4-3) is:

$$COEI = 33.465\ \tau_{co}/\tau_{s\ell,co} + 2.720 \qquad 4\text{-}14$$

with r = .9742.

## C. HCEI Correlation

For the combustor geometry variations with JP 4 (Troth et al., 1973), a reasonable estimate of HCEI can be made from the following equation (Fig. 4-4):

$$HCEI = .0635[COEI(\ell_{hc}/\ell_{co})]^{1.7} \qquad 4\text{-}15$$

where $\ell_{hc} = \ell_{co}$ except for the variable geometry, 0% open configuration (black left pointing triangular symbol). The correlation coefficient for Eq. 4-15 is only .911, most likely due to the scatter exhibited at low HCEI. Since an HCEI of 0.08 corresponds to 1 ppm (as $C_3H_8$) at 100% power, part of this scatter must result from instrumentation difficulties. A characteristic time correlation for HCEI could be attempted, but it is felt that Eq. 4-15 in conjunction with 4-14 is adequate for design purposes. Again, more data are required to characterize cases where $\ell_{hc} \neq \ell_{co}$.

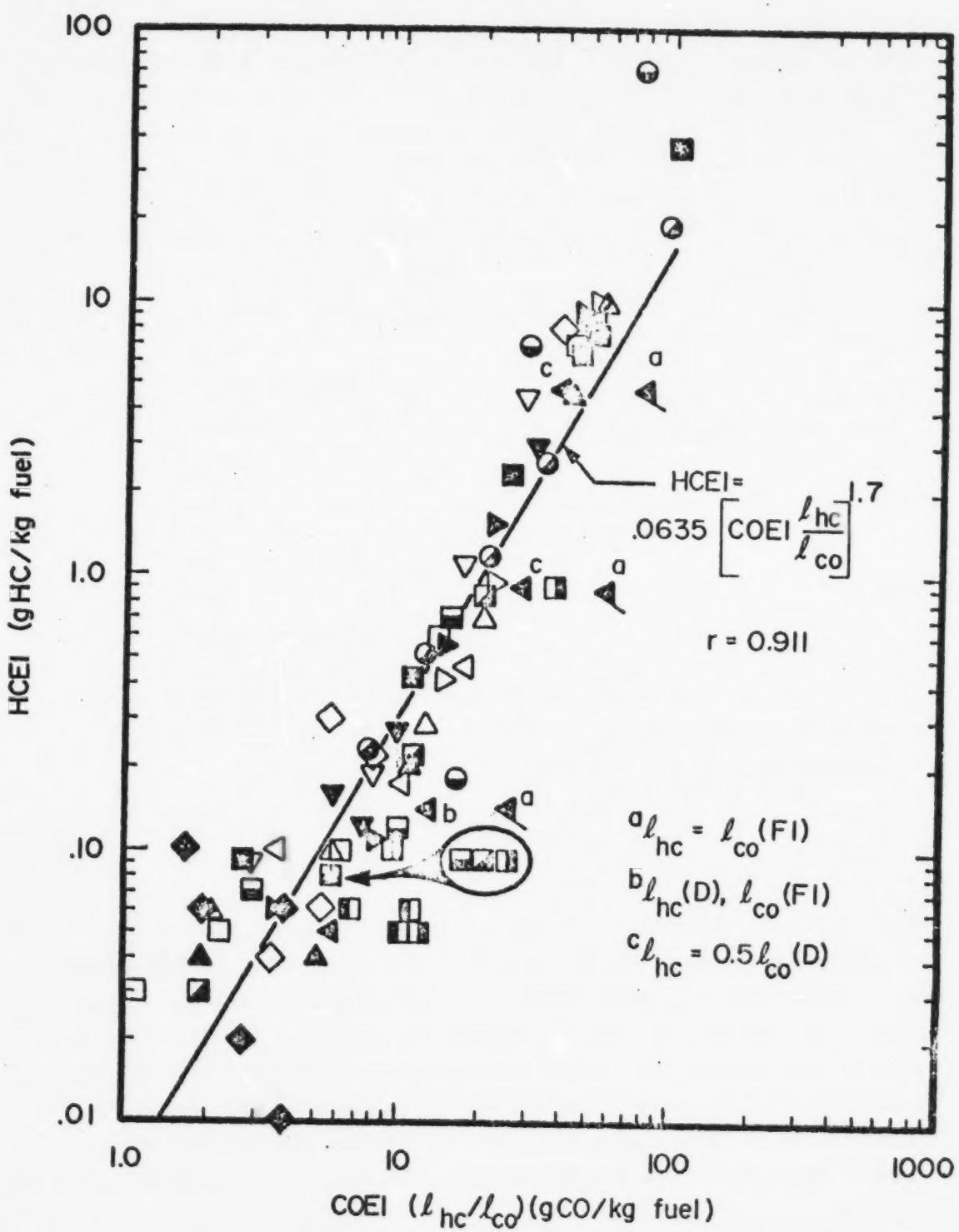


Figure 4-4. Correlation of T-63 HCEI data (from Tuttle et al., 1976).

Inspection of the Allison HCEI (and smoke) data for the air-blast and air-assist injectors shows large variations compared with the pressure atomizing standard nozzle (Troth et al., 1973). In particular HCEI increased and smoke decreased with the use of air for atomization; because insufficient information on nozzle geometries and air flow rates was given, no attempt was made to correlate HCEI in terms of $\tau_{fi}$ (Mellor, 1977b). A preliminary characteristic time model for smoke emissions has only recently been proposed (Dodds et al., 1976).

## D. Advanced Combustors

$NO_x$EI and COEI for the five advanced combustors which deviated significantly from the correlations are plotted versus the appropriate characteristic time ratio in Figures 4-5 and 4-6. The lines on the figures are for Eq. 4-7 and Eq. 4-14, respectively, and may be thought of as defining the emissions from a mixing controlled turbulent diffusion flame combustor at particular values of $\tau_{s\ell,no}/\tau_{no}$ and $\tau_{co}/\tau_{s\ell,co}$.

The goal of advanced combustors is to meet EPA standards (EPA, 1973) and Air Force goals (Blazowski and Henderson, 1972) for aircraft engines. We examine each of the burners listed in Figs. 4-5 and 4-6 from this point of view.

The swirl dome, film injected liner uses wall injection of liquid fuel and replaces the dome of the conventional liners with a large air swirler. Fig. 4-5 shows this configuration to be close to a conventional burner except for high power $NO_x$EI. Perhaps at the air inlet temperatures greater than 515°K (greater than 70% power) some fuel prevaporizing and premixing occurs so that fewer stoichiometric, NO-forming eddies are present per unit fuel injected.

All of the other burners listed in Figs. 4-5 and 4-6 are prechamber combustors, with the flame stabilized in the main chamber via sudden area expansion. The rich premix, swirl version uses the standard injector and is overall rich in the prechamber: it shows excellent reduction in COEI but exhibits conventional $NO_x$EI resulting from the passage of the flow through stoichiometric. Thus this particular type of staged combustion shows no $NO_x$EI advantage. The COEI decrease results from a mechanism other than an $\ell_{co}$ increase (Table 4-4), perhaps prevaporization and premixing.

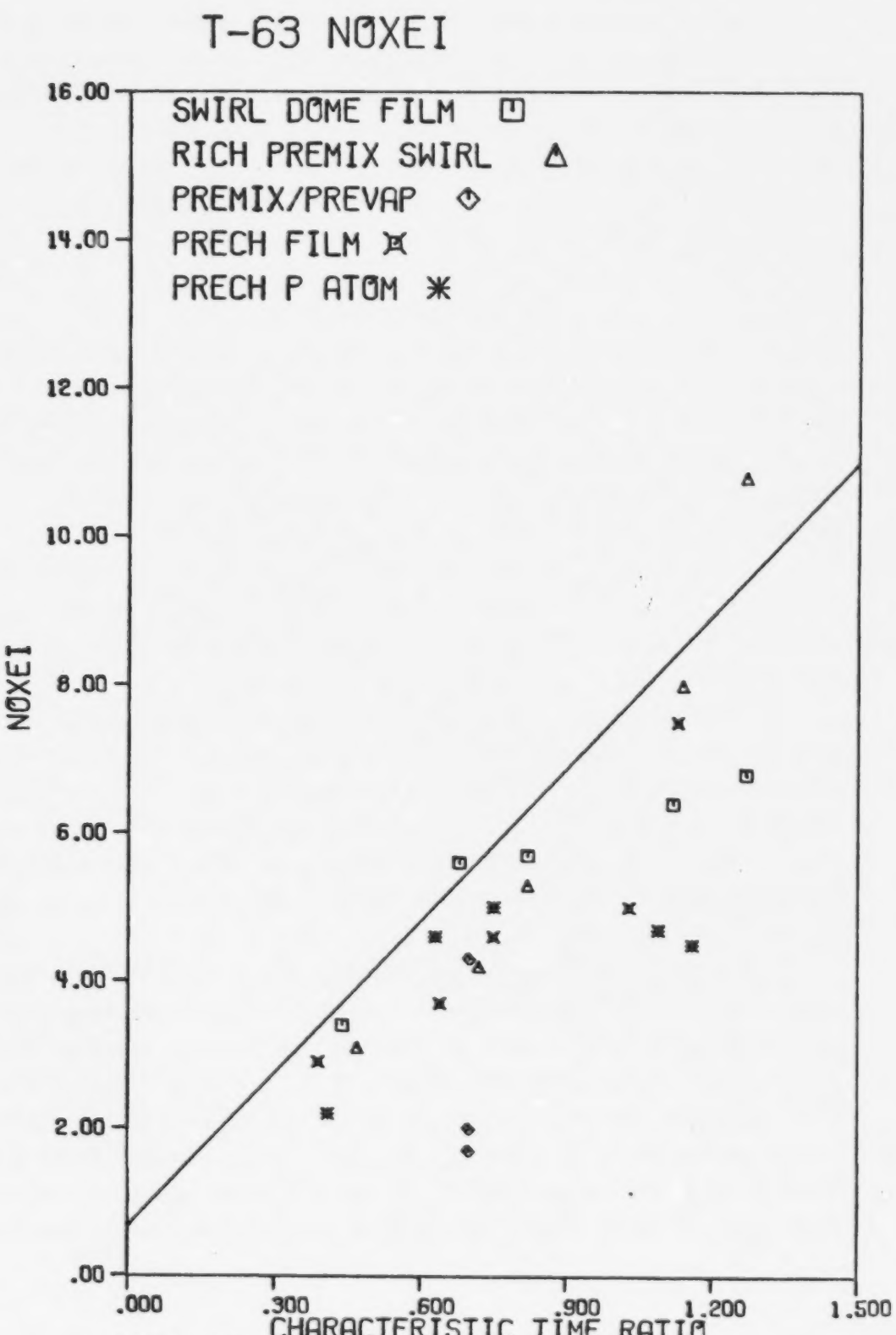


Figure 4-5. $NO_x$EI for advanced T-63 combustors.

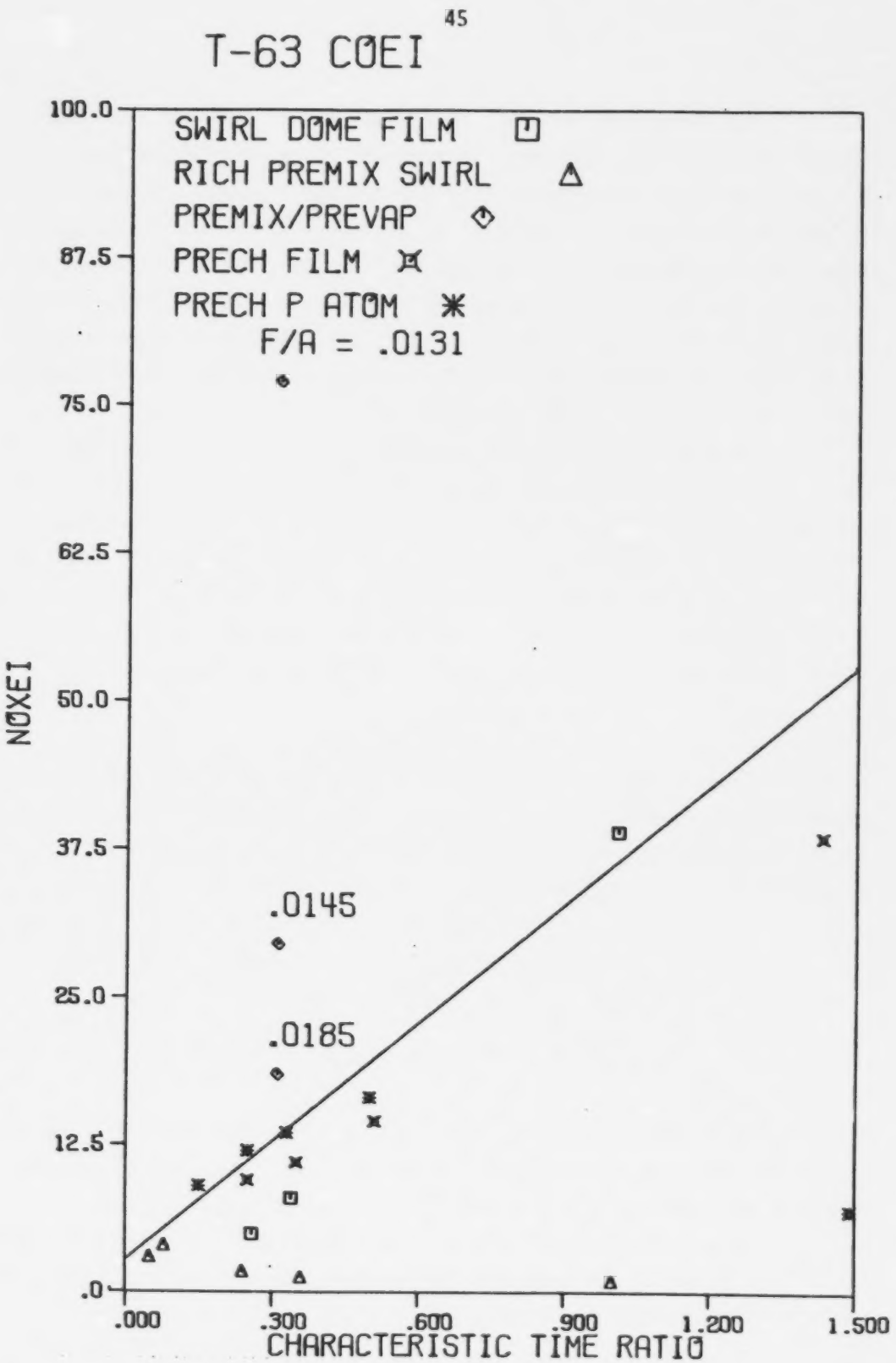


Figure 4-6. COEI for advanced T-63 combustors.

The premix-prevap liner is similar except that the prechamber is overall lean, and emissions are reported for three overall fuel/air ratios at inlet conditions corresponding to the 40% power point. At the highest fuel/air ratio, evidently insufficient prevaporization and premixing can occur with this design since the emissions are very close to conventional. As the fuel/air ratio is decreased the sharp drop in $NO_x$EI shows the prechamber is operating as designed, but at .0131 g f/g air the precipitous increase in COEI reveals the combustor is approaching its lean flammability limit.

The last two prechamber combustors show the difficulty in obtaining prevaporization and premixing over the entire engine load range. Prech, film utilizes wall fuel injection, while prech, p atom uses conventional atomization. At some power points in Figs. 4-5 and 4-6 the low $NO_x$EI and COEI compared to conventional demonstrate some prevaporizing and premixing is obtained, but the other power points exhibit conventional emissions. Thus much additional work is required on this type of burner.

## E. Summary

Characteristic time parameters have been used to correlate emissions for the T-63 helicopter combustor. Effects of fuel type, atomization, and combustor geometry are considered and the results for systems with negligible droplet lifetimes are

$$NO_x EI = 6.882\ \tau_{s\ell,no}/\tau_{no} + 0.686 \qquad 4\text{-}7$$

$$COEI = 33.465\ \tau_{co}/\tau_{s\ell,co} + 2.720 \qquad 4\text{-}14$$

Also, Fig. 4-4 shows a correlation of HCEI versus COEI, demonstrating that, so long as COEI can be correlated in terms of fuel, run conditions, etc., an independent correlation for HCEI is probably not necessary.

Advanced combustors are also considered in subsection 4-D. Figs. 4-5 and 4-6 show how the emissions levels from these designs compare with those for the conventional burners.

# V. CHARACTERISTIC TIME STUDIES ON THE JT9D COMBUSTOR

In this section characteristic time parameters will be used to correlate nitric oxides and carbon monoxide for the JT9D combustor. The effect of variations in ambient conditions on nitric oxides will also be considered.

The JT9D is an annular, swirl-stabilized, aircraft gas turbine combustor manufactured by Pratt and Whitney Aircraft Company; a half-section is shown in Fig. 5-1. Pratt and Whitney supplied data (Nelson, 1976) consisting of 270 engine run points for three burner modifications (II, III, and V). Air-addition hole placements and sizes were almost identical for the three burners; Sturgess (1978) indicates that dome designs and swirl angles (45°) are the same for the modifications considered.

Because the JT9D differs significantly from the previous burners investigated, it was chosen for analysis. The first difference is that the JT9D is much larger than either the GT-309 or the T-63 with an outer diameter of approximately 98 centimeters as compared to 19.04 and to 13.81, respectively. Next, the JT9D is an annular design rather than a can configuration. Third, this burner is swirl-stabilized instead of jet stabilized. Finally, the JT9D potentially will produce more pollution because of its greater fuel consumption rate; for these reasons, characteristic time studies were extended to this combustor.

In a similar matter as for the GT-309 and the T-63, discussions of a nitric oxides correlation and a carbon monoxide correlation for the JT9D follow. After these, the effect of ambient humidity, temperature, and pressure on nitric oxides will be examined.

## A. Nitric Oxides Correlation

The terms used in the JT9D nitric oxides correlation are almost the same as those used in the same correlation for the GT-309 and the T-63:

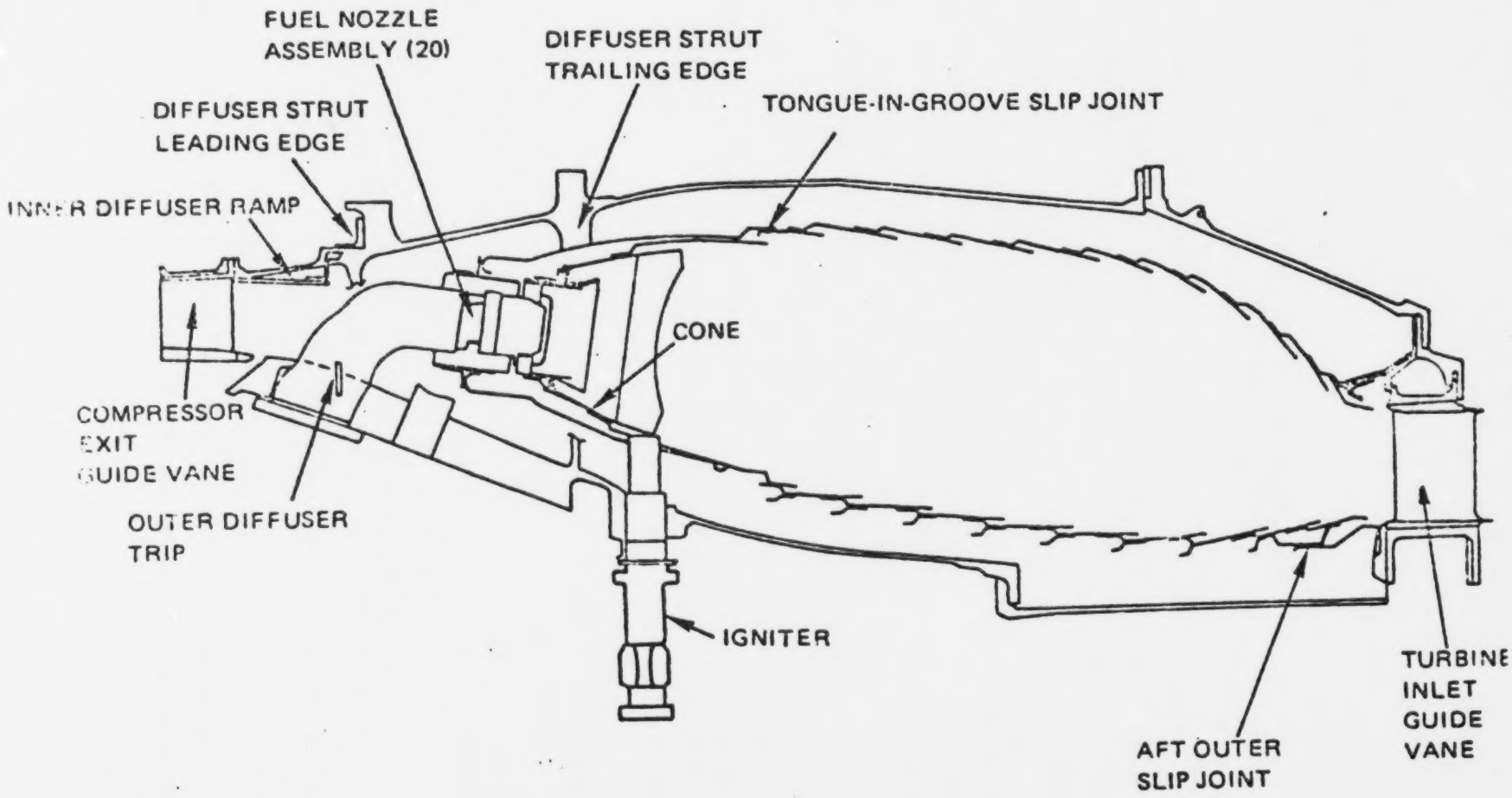


Figure 5-1. Half section of the JT9D combustor.

$$\tau_{no} = 10^{-12}\exp(135/RT_{\phi=1}) \qquad 5\text{-}1$$

$$\tau_{s\ell,no} = \ell_{no}/V_{\phi=1} \qquad 5\text{-}2$$

$$\ell_{no}^{-1} = \ell_{quench}^{-1} + [(r_{outer} - r_{inner})]^{-1} \qquad 5\text{-}3$$

$$V_{\phi=1} = (fs)\dot{m}_a\, RT_{\phi=1}/PM\tfrac{\pi}{4}(d_{outer}^2 - d_{inner}^2) \qquad 5\text{-}4$$

The only difference between these terms and those used previously is the diameter chosen; the gap in the annulus is used instead of the combustor's outer diameter. Notice that through this choice the combustor is, in effect, viewed as twenty smaller combustors of the diameter

$$d = r_{outer} - r_{inner} \qquad 5\text{-}5$$

There are twenty combustors because, as Fig. 5-1 shows, there are twenty fuel injection sites. As in the previous cases the reference area is used in the velocity term (5-4). In Eq. 5-4, for all points,

$$\ell_{quench} = \ell_{sec}$$

where $\ell_{sec}$ is the axial length to the secondary air addition holes; in Eq. 5-4 the flow split fractions (fs) are

| Mod | (fs) |
|---|---|
| II | 0.428 |
| III | 0.456 |
| V | 0.454 |

The resulting correlation (shown in Fig. 5-2) is

$$NO_x EI = 5.326\ \tau_{s\ell,no}/\tau_{no} - 1.089 \qquad 5\text{-}6$$

with r = .9502. All 270 points were included in the correlation.

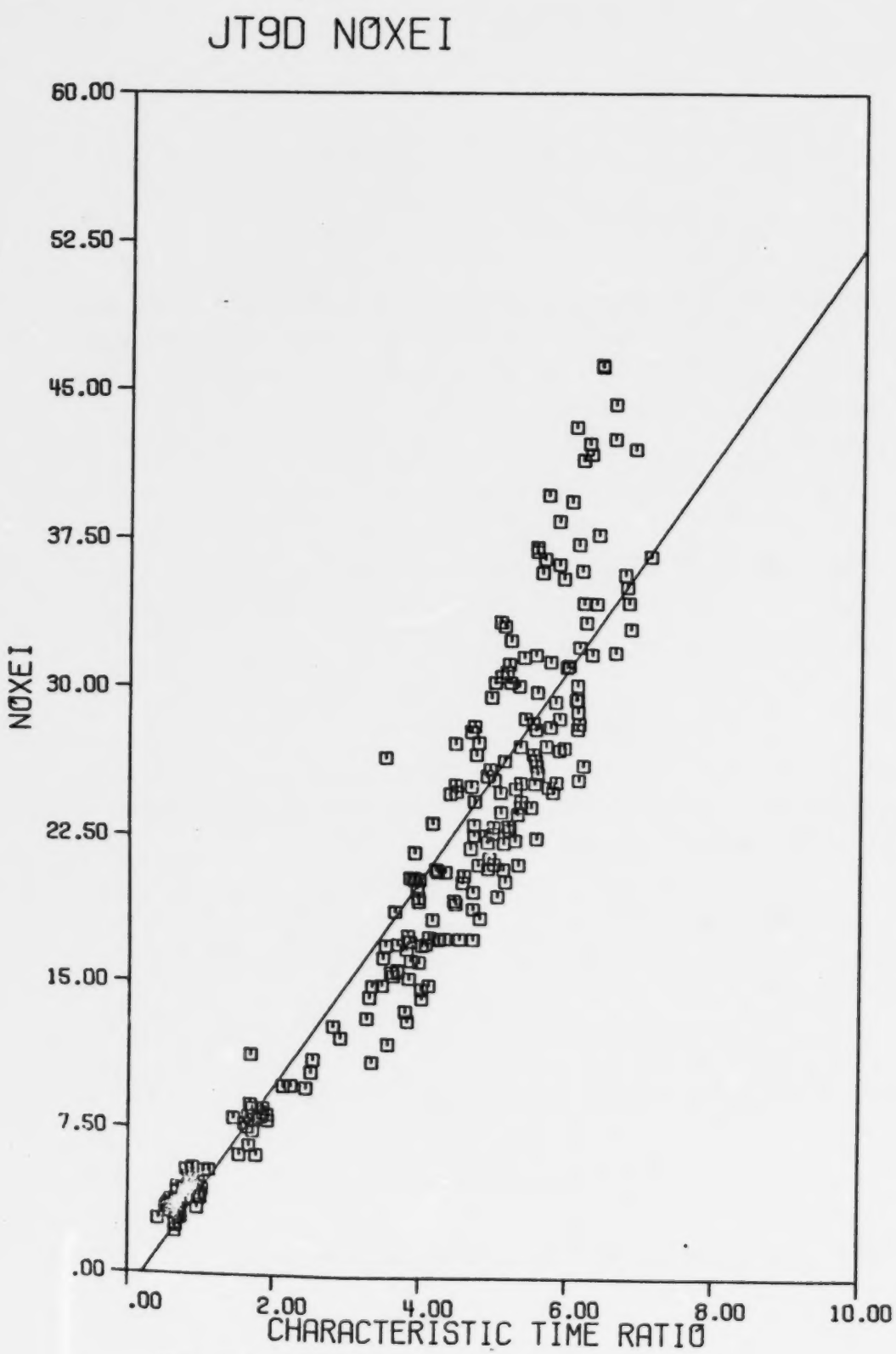


Figure 5-2. Correlation of the JT9D $NO_x$EI data.

But the above analysis ignores swirl; how can this effect be accounted for? With a swirler operating, a fuel particle traveling down the burner should, to some extent, tend to follow a spiral; this will tend to increase the distance the particle travels. We approximate this distance by

$$\ell_{quench} = \ell_{quench,no\ swirl}/\cos\theta \qquad 5\text{-}7$$

where $\theta$ is the swirl angle. For the present case

$$\ell_{quench} = \ell_{sec} \qquad 5\text{-}8$$

Using Eqs. 5-1, 5-2, 5-3 again, the resulting correlation is

$$NO_xEI = 4.713\ \tau_{s\ell,no}/\tau_{no} - 1.089 \qquad 5\text{-}9$$

with r = .9502.

B. Carbon Monoxide Correlation

The terms used in the JT9D carbon monoxide correlation are

$$\tau_{co} = 10^{-3}\exp(10.76/RT_{avg}) \qquad 5\text{-}10$$

$$T_{avg} = (T_{in} + T_{out})/2 \qquad 5\text{-}11$$

$$\tau_{s\ell,co} = \ell_{co}/V_{ref} \qquad 5\text{-}12$$

$$\ell_{co}^{-1} = \ell_{quench}^{-1} + [(r_{outer} - r_{inner})]^{-1} \qquad 5\text{-}13$$

$$V_{ref} = \dot{m}_a RT_{in}/PM\frac{\pi}{4}(d_{outer}^2 - d_{inner}^2) \qquad 5\text{-}14$$

Except for the diameter difference noted earlier in this section, the terms (neglecting swirl) are the same as those used in the GT-309 and the T-63 carbon monoxide correlations.

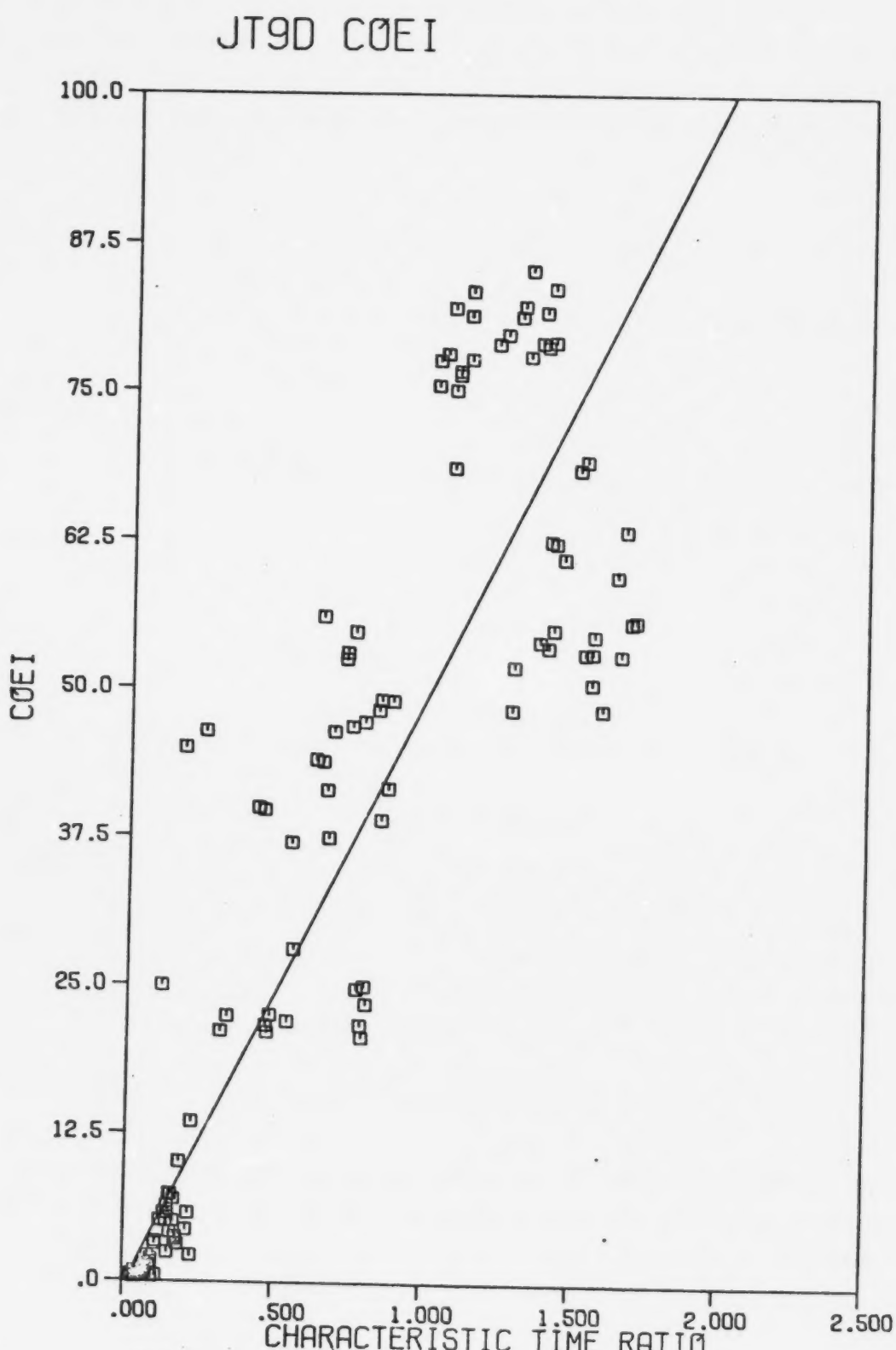


Figure 5-3. Correlation of the JT9D COEI data.

Only the length to the primary holes, the length to the secondary holes, and the difference between these lengths were considered for the quench lengths. This is because, while there are numerous other air-addition sites on the liner, only the primary and the secondary holes contribute a large enough fraction of the total flow to be likely to affect the oxidation of carbon monoxide. Then the best combination of lengths is chosen by a computer program.

The resulting correlation (shown in Fig. 5-3) is

$$COEI = 49.846\ \tau_{co}/\tau_{co,s\ell} - 0.572 \qquad 5\text{-}15$$

with r = .9301.

To include a swirl effect, the lengths used for Eq. 5-15 are modified via Eq. 5-7 and the computer program used again to determine the best combination of values for the fit. The resulting correlation is

$$COEI = 58.976\ \tau_{co}/\tau_{s\ell,co} - 0.668 \qquad 5\text{-}16$$

with r = .9310.

### C. Ambient Effects on Nitric Oxides

Emissions of oxides of nitrogen from conventional gas turbine engines are highly sensitive to the engine (and thus combustor) inlet air quality: minor changes in water content, air temperature, and pressure create sizable variations in the peak combustion temperature, upon which $NO_x$ has a high functional dependence. A review of ambient effect findings from the literature follows, along with a summary of a correlation technique capable of removing this dependence, with examples taken from JT9D engine certification tests.

The review of the literature revealed that the following consequences of ambient variations were predicted for conventional gas turbines operating at representative conditions. Lipfert (1972) reduced scatter significantly by decreasing $NO_x$EI by 20 percent for each 0.01 (by weight) of water vapor in excess of 0.01 specific humidity. More directly, Carl (1974) in relating the fraction ($NO_x$ at ambient humidity) with respect to

the ($NO_x$ level at a specific humidity of 0.005) versus percent specific humidity obtained a straight line with a slope of -10.7 percent. In addition, it was suggested that ambient humidity had 60.7 percent the effect of water injection; thus for a similar correlation in terms of water injection, a slope of -17.6 percent results. Finally, in a theoretical fashion, Blazowski, Walsh, and Mach (1975) produced a chart demonstrating the humidity effect on nitric oxides emission levels.

In considering ambient temperature effects, Blazowski et al. developed a theoretical correction factor and expressed it in the form of a graph for pressure ratios of ten to twenty-five and stoichiometric ratios of 0.6 to 0.9.

In reviewing the conclusions reached on the effect of combustor inlet pressure variations on nitric oxides emission levels, the consensus was that from kinetic considerations along (constant reference velocity)

$$NO_x \sim P^a \qquad 5\text{-}17$$

Fenimore's (1970) results were consistent with this where a equaled 0.5 $\pm$ 0.1. Likewise, Vermes (1974) used the above relation with a = 0.5 for correlating $NO_x$. From an experimental analysis on swirl-can combustors, Mularz, Wear, and Verbulecz (1975) found that the exponent varied from 0.13 to 0.74.

Recalling that

$$NO_xEI \sim \tau_{s\ell,no}/\tau_{no} \qquad 5\text{-}18$$

where the parameters are defined in Eqs. 5-1, 5-2, 5-3, and 5-4, Eq. 5-18 will allow the inclusion of ambient effects: we consider each separately below.

The presence of <u>water vapor</u> will have its most significant effect upon the computed adiabatic stoichiometric flame temperature $T_{\phi=1}$, with this temperature (and thus $NO_xEI$) decreasing as ambient humidity increases, since the inverse linear dependence (in $V_{\phi=1}$) in $\tau_{s\ell,no}$ will be overpowered by the exponential dependence in $\tau_{no}$.

<u>Ambient air temperature</u> has a similar effect upon combustor inlet temperature and thus $T_{\phi=1}$: again increases in ambient temperature increase $T_{\phi=1}$ and $NO_xEI$ through the exponential dependence in the kinetic time.

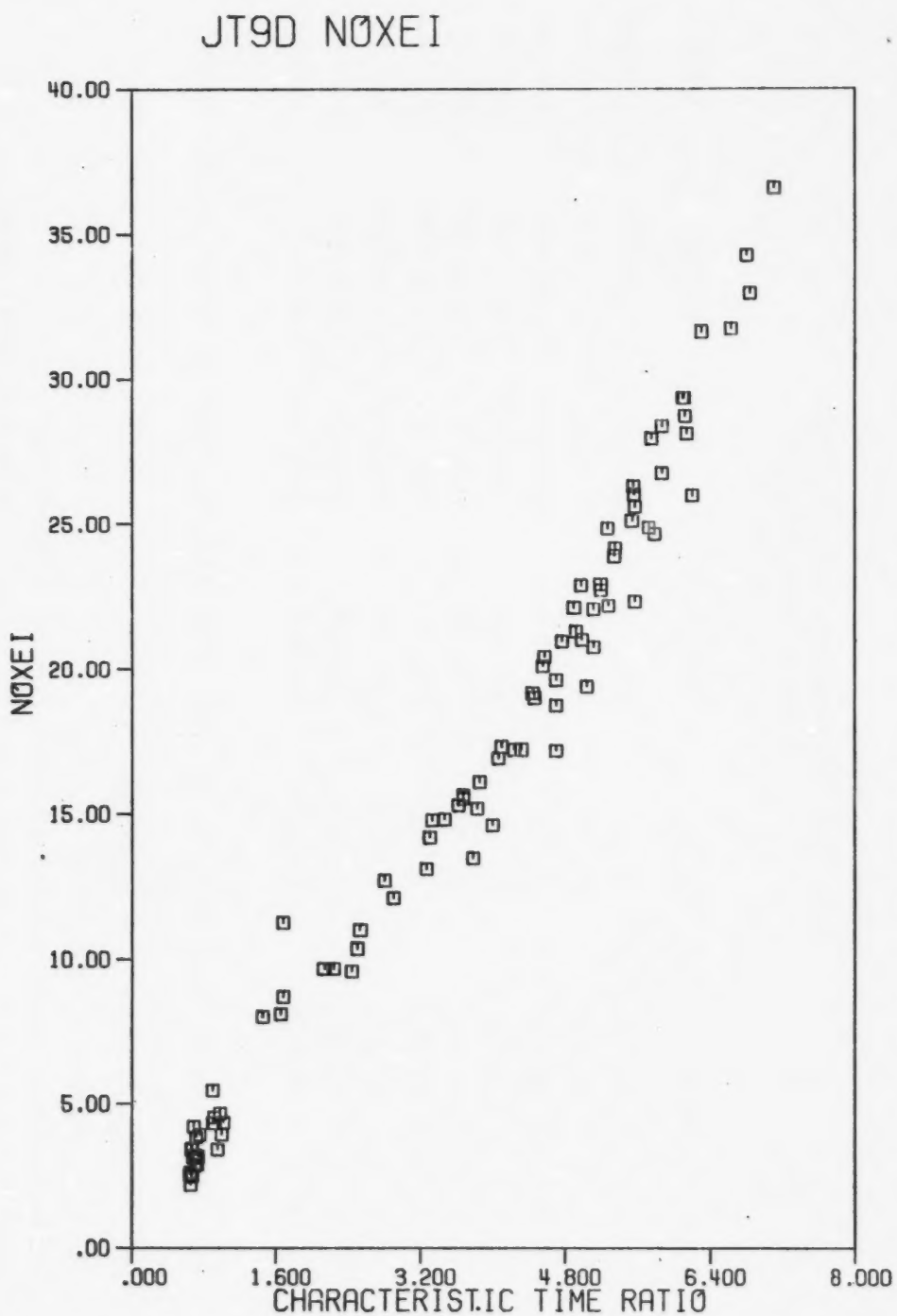


Figure 5-4. Correlation of the JT9D $NO_x$EI data for one burner modification with one fuel.

Table 5-1. Temperatures Calculated With Measured Inlet Conditions (.0073 g $H_2$)/g air)

| POWER | MADT(KG/SEC) | P(ATM) | TI(K) | TA(K) | TEXH(K) | TSTO(K) |
|---|---|---|---|---|---|---|
| 1 | 20.714 | 3.468 | 465.333 | 671.167 | 877.000 | 2368.000 |
| 2 | 21.988 | 3.687 | 470.889 | 670.444 | 870.000 | 2374.000 |
| 3 | 49.136 | 9.669 | 629.889 | 908.994 | 1188.000 | 2471.000 |
| 4 | 58.412 | 11.909 | 669.000 | 983.000 | 1297.000 | 2495.000 |
| 5 | 70.662 | 14.706 | 709.500 | 1030.750 | 1352.000 | 2520.000 |
| 6 | 78.957 | 16.838 | 736.722 | 1082.361 | 1428.000 | 2537.000 |
| 7 | 82.375 | 17.750 | 747.111 | 1102.556 | 1458.000 | 2544.000 |
| 8 | 85.703 | 18.653 | 756.000 | 1122.500 | 1489.000 | 2550.000 |
| 9 | 90.019 | 19.940 | 771.611 | 1157.306 | 1543.000 | 2559.000 |

MADT = burner air mass flow rate (computed from fuel flow rate and burner fuel/air ratio)
P = burner inlet pressure
TI = burner inlet air temperature
TA = average of TI and TEXH
TEXH = burner outlet temperature (from chemical equilibrium)
TSTO = adiabatic stoichiometric flame temperature (from chemical equilibrium)

Lowest fuel flow rate is arbitrarily labeled power 1.

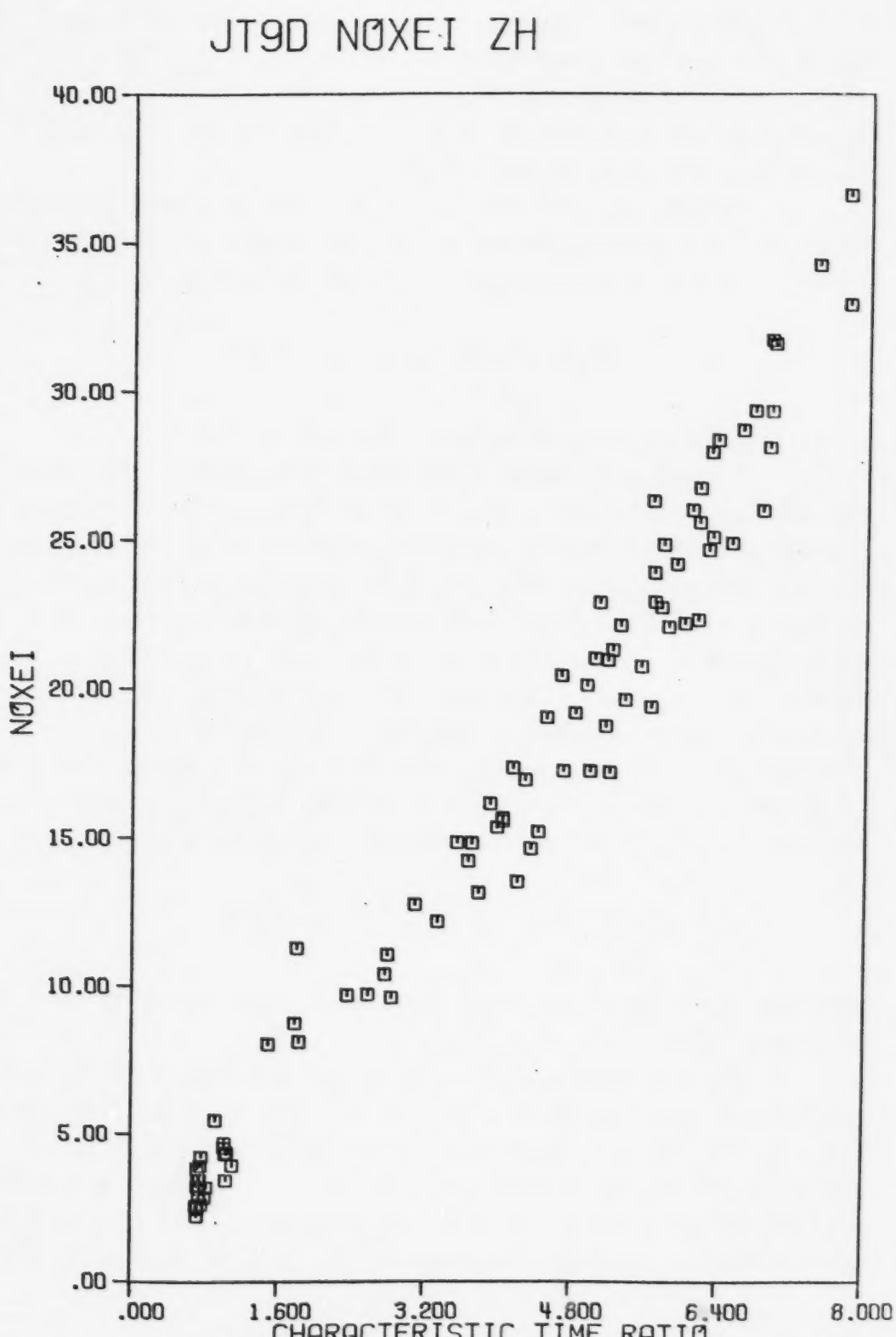


Figure 5-5. Correlation of the JT9D $NO_X$EI data for one burner modification with one fuel and neglecting ambient humidity.

Any change in ambient pressure is reflected in the value of combustor inlet pressure appearing in Eq. 5-4 for $V_{\phi=1}$. $NO_x EI$ is a direct function of P. A second order effect is that increases in P also increase $T_{\phi=1}$ through the suppression of equilibrium dissociation; as noted previously this also leads to higher $NO_x EI$.

Data for one JT9D modification were used for sample calculations on the effect of ambient variations; the least squares fit for these data (shown in Fig. 5-4), including all day to day variations, is

$$NO_x EI = 4.554\ \tau_{s\ell,no}/\tau_{no} - 0.409 \qquad 5\text{-}19$$

with a standard deviation in slope of .080 and r = .987.

A sample calculation of the effect of humidity is shown in Tables 5-1 and 5-2 for one engine. The data in the former table are shown in Fig. 5-3 with the other engine data and were computed with the actual specific humidity (approximately 0.0073 g $H_2O$/g air) measured by Pratt and Whitney. In Table 5-2 the flame temperatures assuming no water vapor present in the inlet air are presented. The effect of the triatomic $H_2O$ replacing the diatomic $N_2$ in the air is the lower TSTO ($T_{\phi=1}$) in Table 5-1, about a 13°K decrease. Similar calculations have been performed for all engines of Fig. 5-4 with the result shown in Fig. 5-5. As can be seen the scatter is increased (standard deviation in slope to .082), and the correlation coefficient r has decreased to .983. The least squares fit equation for Fig. 5-5 is

$$NO_x EI = 4.133\ \tau_{s\ell,no}/\tau_{no} - 0.272 \qquad 5\text{-}20$$

where the slope change from Eq. 5-19 reflects correlation of the same data with lower values of $\tau_{no}$.

For ascertaining ambient temperature and pressure effects a different approach was used. One engine, actually tested at 294°K and 0.99 atm, was selected, with baseline temperatures calculated as shown in Table 5-3. For the same pressure, engine inlet temperatures of 244 and 322°K were taken, with the results shown in Tables 5-4 and 5-5, respectively (TI's were computed assuming a polytropic compression). For each of these new burner inlet

Table 5-2. Temperatures Calculated Assuming Zero Humidity

| POWER | MADT(KG/SEC) | P(ATM) | TI(K) | TA(K) | TEXH(K) | TSTO(K) |
|---|---|---|---|---|---|---|
| 1 | 20.714 | 3.468 | 465.333 | 672.667 | 880.000 | 2382.000 |
| 2 | 21.988 | 3.687 | 470.889 | 671.444 | 872.000 | 2386.000 |
| 3 | 49.136 | 9.669 | 629.889 | 910.444 | 1191.000 | 2485.000 |
| 4 | 58.412 | 11.909 | 669.000 | 985.500 | 1302.000 | 2509.000 |
| 5 | 70.662 | 14.706 | 709.500 | 1032.750 | 1356.000 | 2534.000 |
| 6 | 78.957 | 16.838 | 736.722 | 1084.861 | 1433.000 | 2550.000 |
| 7 | 82.375 | 17.750 | 747.111 | 1105.056 | 1463.000 | 2557.000 |
| 8 | 85.703 | 18.653 | 756.000 | 1125.000 | 1494.000 | 2562.000 |
| 9 | 90.019 | 19.940 | 771.611 | 1159.806 | 1548.000 | 2572.000 |

Table 5-3. Baseline Temperatures, Engine P896, Computed with Measured Inlet Conditions (294°K, 0.99 atm)

| POWER | MADT(KG/SEC) | P(ATM) | TI(K) | TA(K) | TEXH(K) | TSTO(K) |
|---|---|---|---|---|---|---|
| 1 | 21.252 | 3.519 | 462.667 | 667.333 | 872.000 | 2371.000 |
| 2 | 21.624 | 3.576 | 465.389 | 667.694 | 870.000 | 2374.000 |
| 3 | 22.512 | 3.762 | 474.833 | 671.417 | 868.000 | 2378.000 |
| 4 | 50.775 | 9.927 | 627.333 | 907.667 | 1188.000 | 2475.000 |
| 5 | 59.409 | 12.118 | 664.222 | 977.611 | 1291.000 | 2497.000 |
| 6 | 80.594 | 17.086 | 732.389 | 1076.694 | 1421.000 | 2539.000 |
| 7 | 84.230 | 18.049 | 740.222 | 1096.111 | 1452.000 | 2545.000 |
| 8 | 87.770 | 19.042 | 755.444 | 1124.222 | 1493.000 | 2553.000 |
| 9 | 91.922 | 20.326 | 771.278 | 1162.139 | 1553.000 | 2563.000 |

Table 5-4. Temperatures, Engine P896,
Computed for 244°K, 0.99 atm

| POWER | MADT(KG/SEC) | P(ATM) | TI(K) | TA(K) | TEXH(K) | TSTO(K) |
|---|---|---|---|---|---|---|
| 1 | 21.252 | 3.519 | 383.778 | 592.889 | 802.000 | 2337.000 |
| 2 | 21.624 | 3.576 | 386.222 | 592.611 | 799.000 | 2339.000 |
| 3 | 22.512 | 3.762 | 393.556 | 594.278 | 795.000 | 2342.000 |
| 4 | 50.775 | 9.927 | 523.111 | 810.556 | 1098.000 | 2427.000 |
| 5 | 59.409 | 12.118 | 554.889 | 876.944 | 1199.000 | 2447.000 |
| 6 | 80.594 | 17.086 | 608.667 | 963.333 | 1318.000 | 2481.000 |
| 7 | 84.230 | 18.049 | 613.556 | 980.278 | 1347.000 | 2485.000 |
| 8 | 87.770 | 19.042 | 628.222 | 1007.611 | 1387.000 | 2493.000 |
| 9 | 91.922 | 20.326 | 640.444 | 1042.722 | 1445.000 | 2501.000 |

Table 5-5. Temperatures, Engine P896,
Computed for 322°K, 0.99 atm

| POWER | MADT(KG/SEC) | P(ATM) | TI(K) | TA(K) | TEXH(K) | TSTO(K) |
|---|---|---|---|---|---|---|
| 1 | 21.252 | 3.519 | 505.889 | 708.444 | 911.000 | 2390.000 |
| 2 | 21.624 | 3.576 | 509.111 | 709.056 | 909.000 | 2393.000 |
| 3 | 22.512 | 3.762 | 518.778 | 712.889 | 907.000 | 2397.000 |
| 4 | 50.775 | 9.927 | 689.556 | 965.778 | 1242.000 | 2503.000 |
| 5 | 59.409 | 12.118 | 731.444 | 1040.222 | 1349.000 | 2528.000 |
| 6 | 80.594 | 17.086 | 802.333 | 1141.167 | 1480.000 | 2572.000 |
| 7 | 84.230 | 18.049 | 808.778 | 1159.389 | 1510.000 | 2577.000 |
| 8 | 87.770 | 19.042 | 828.111 | 1190.556 | 1553.000 | 2587.000 |
| 9 | 91.922 | 20.326 | 844.222 | 1228.611 | 1613.000 | 2597.000 |

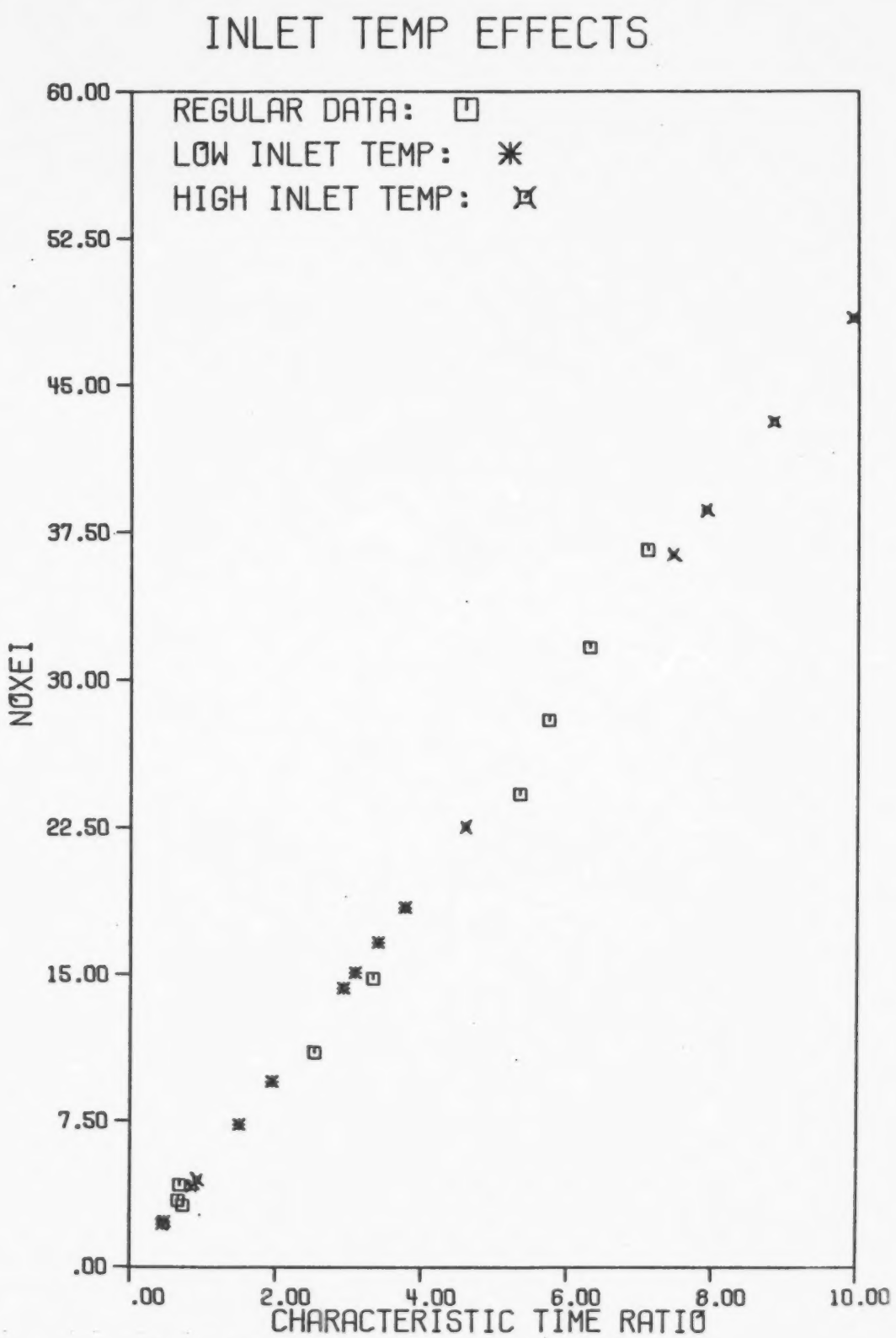


Figure 5-6. Ambient temperature effect on $NO_x$EI.

Table 5-6. Temperatures, Engine P896
Computed for 294°K, 0.95 atm

| POWER | MADT(KG/SEC) | P(ATM) | TI(K) | TA(K) | TEXH(K) | TSTO(K) |
|---|---|---|---|---|---|---|
| 1 | 21.252 | 3.352 | 462.667 | 667.333 | 872.000 | 2370.000 |
| 2 | 21.624 | 3.410 | 465.389 | 667.694 | 870.000 | 2372.000 |
| 3 | 22.512 | 3.582 | 474.833 | 671.417 | 868.000 | 2377.000 |
| 4 | 50.775 | 9.486 | 627.333 | 907.667 | 1188.000 | 2473.000 |
| 5 | 59.409 | 11.600 | 664.222 | 977.611 | 1291.000 | 2496.000 |
| 6 | 80.594 | 15.739 | 732.389 | 1076.694 | 1421.000 | 2537.000 |
| 7 | 84.230 | 17.362 | 740.222 | 1096.111 | 1452.000 | 2544.000 |
| 8 | 87.770 | 18.333 | 755.444 | 1124.222 | 1493.000 | 2552.000 |
| 9 | 91.922 | 19.590 | 771.278 | 1162.139 | 1553.000 | 2562.000 |



Table 5-7. Temperatures, Engine P896,
Computed for 294°K, 1.05 atm

| POWER | MADT(KG/SEC) | P(ATM) | TI(K) | TA(K) | TEXH(K) | TSTO(K) |
|---|---|---|---|---|---|---|
| 1 | 21.252 | 3.688 | 462.667 | 667.333 | 872.000 | 2373.000 |
| 2 | 21.624 | 3.750 | 465.389 | 667.694 | 870.000 | 2375.000 |
| 3 | 22.512 | 3.940 | 474.833 | 671.417 | 868.000 | 2379.000 |
| 4 | 50.775 | 10.434 | 627.333 | 907.667 | 1188.000 | 2476.000 |
| 5 | 59.409 | 12.760 | 664.222 | 977.611 | 1291.000 | 2499.000 |
| 6 | 80.594 | 18.061 | 732.389 | 1076.694 | 1421.000 | 2541.000 |
| 7 | 84.230 | 19.098 | 740.222 | 1096.111 | 1452.000 | 2546.000 |
| 8 | 87.770 | 20.167 | 755.444 | 1124.222 | 1493.000 | 2555.000 |
| 9 | 91.922 | 21.550 | 771.278 | 1162.139 | 1553.000 | 2566.000 |

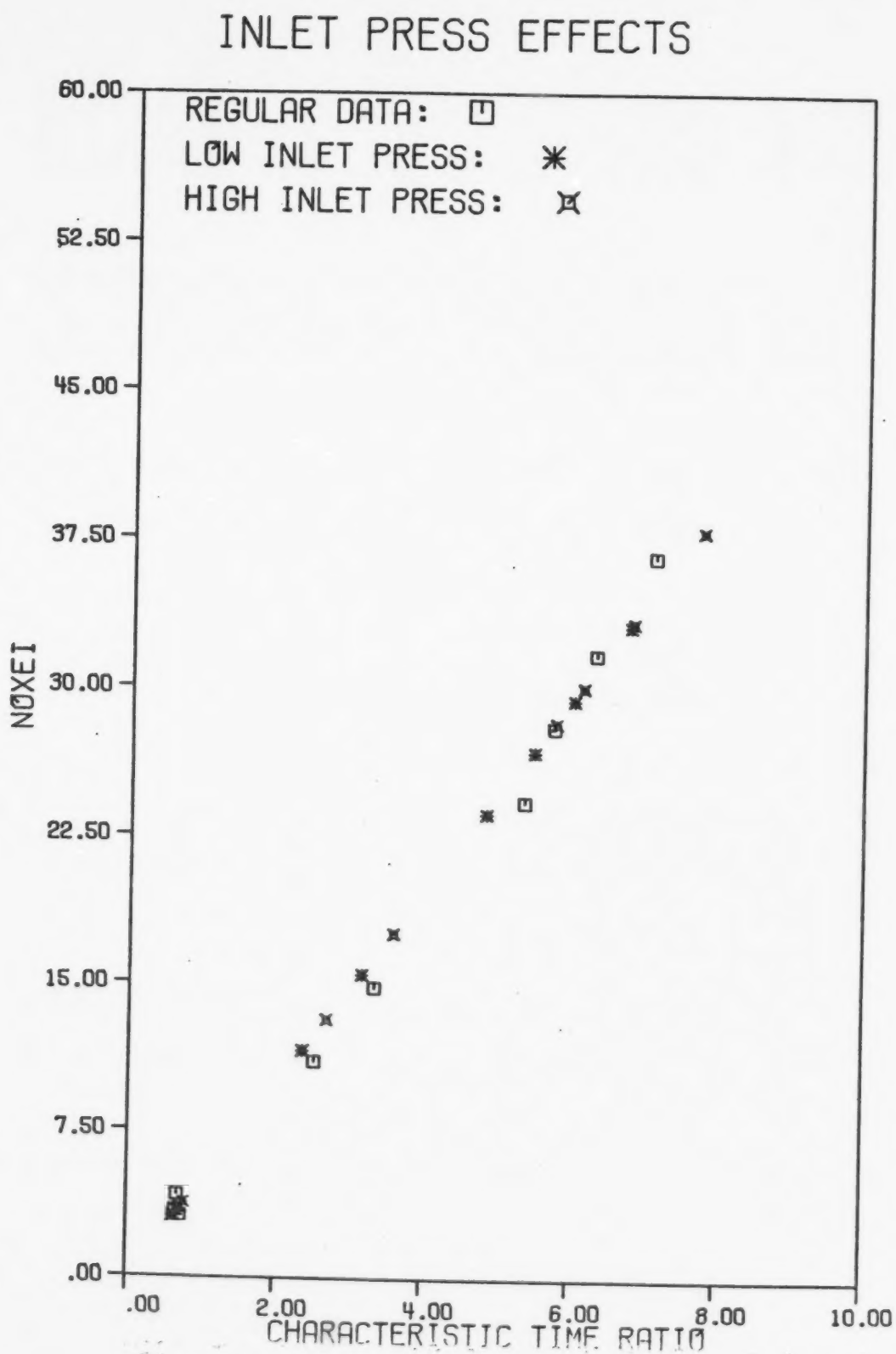


Figure 5-7. Ambient pressure effect on $NO_xEI$.

air temperatures and new adiabatic stoichiometric flame temperatures, Eq. 5-19 was used to compute the resulting $NO_x EI$: Fig. 5-6 shows the significant changes which result from variations in ambient air temperature, compared with the baseline data obtained on a nearly standard day.

A similar method was utilized for ambient pressure. For the same engine, air temperature was held constant at 294°K, but inlet pressure was taken as 0.95 or 1.05 atm (baseline was 0.99 atm). The accompanying changes in burner inlet pressure and TSTO are listed in Tables 5-6 and 5-7; note that the primary effect is on P rather than TSTO, as noted previously. Fig. 5-7 shows the computed changes in $NO_x EI$. Note that the model predicts a complicated pressure scaling parameter:

$$NO_x EI \sim P/T_{\phi=1}\ \tau_{no} \qquad 5\text{-}21$$

Again the exponential dependence of $\tau_{no}$ will overcome the linear $T_{\phi=1}$ term, so as pressure and $T_{\phi=1}$ increase, $\tau_{no}$ decreases, which suggests a greater than unity exponent (when including the variation in reference velocity with pressure).

As an additional note, humidity effects were analyzed and a semi-empirical correction factor developed for the specific case of the JT9D combustor. This was done in the following manner: the specific humidity levels of the JT9D data supplied were assumed to be equal to zero and values of the resulting characteristic time ratio then calculated; next the corresponding magnitudes of $NO_x EI$ were predicted using Eq. 5-19; finally by checking the variation of $NO_x EI$ with respect to specific humidity levels, a correlation was found. $NO_x EI$ decreased by approximately twenty percent for each one percent increase in specific humidity; this represents a value of -20 percent for the correction factor.

This JT9D humidity correction factor of -20 percent agrees quite well with the literature. The magnitude of the factor is the same as the humidity correction used by Lipfert and close to Carl's result for water injection. In addition, for the appropriate operating pressure ratios the correction factor is compatible with the predictions of Blazowski et al. However, the factor was developed for the JT9D and does not necessarily apply for other engines.

In comparing the ambient pressure scaling results predicted by the model with the findings in the literature, there is an apparent discrepancy. The model suggests that the exponential dependency of $NO_x EI$ on pressure is of the first order, while the literature suggests that the exponent's value is around one-half. However, the exponent of one-half is a result of kinetic considerations only, whereas the model predicts pressure effects on reference velocity and the related variance of $NO_x EI$.

## D. Summary

Emissions for the JT9D combustor have been correlated using characteristic time parameters. Neglecting swirl effects, the correlations for nitric oxides and carbon monoxide are

$$NO_x EI = 5.326\ \tau_{s\ell,no}/\tau_{no} - 1.089 \qquad 5\text{-}6$$

$$COEI = 49.846\ \tau_{co}/\tau_{s\ell,co} - 0.572 \qquad 5\text{-}15$$

respectively. When a swirl effect is introduced these least squares fit change to

$$NO_x EI = 4.713\ \tau_{s\ell,no}/\tau_{no} - 1.089 \qquad 5\text{-}9$$

$$COEI = 58.976\ \tau_{co}/\tau_{s\ell,co} - 0.668 \qquad 5\text{-}16$$

respectively.

In subsection C, the ambient effects on nitric oxides are analyzed; the following scaling parameter is recommended

$$NO_x EI \sim P \exp(-67.976/T_{\phi=1})/T_{\phi=1} \qquad 5\text{-}22$$

Here P is combustor inlet pressure, and $T_{\phi=1}$(°K) is the adiabatic stoichiometric flame temperature (a function of ambient air properties and fuel heating value), computed assuming chemical equilibrium. Since Eq. 5-22 is derivable from first principles, it may yield better correlations than purely empirical relations and should apply to any engine at any pressure ratio.

# VI. CONCLUSIONS

A physical model of spray combustion has been used to correlate emissions from conventional gas turbines. The dominant subprocesses in these devices have been expressed in terms of times and then these times used to form dimensionless correlation parameters for emissions species. Generally, heterogeneous effects have been assumed negligible and only nitric oxides and carbon monoxides have been correlated.

As stated in the introduction, universal correlations are sought for design purposes; below, the data for the three combustors analyzed will be correlated together and examined in terms of a universal correlation.

## A. Nitric Oxides

The combined $NO_x EI$ data for the GT-309, the T-63, and the JT9D were correlated; the least squares fit (shown in Fig. 6-1) is

$$NO_x EI = 4.821\ \tau_{s\ell,no}/\tau_{no} + 0.687 \qquad 6\text{-}1$$

with a correlation coefficient (r) of .9435. This correlation consists of the data that assume no reverse flow effect and no swirl effect. Table 6-1 shows the individual $NO_x$ correlations.

Table 6-1. Constants for $NO_x EI = A\tau_{s\ell,no}/\tau_{no} + B$

| Engine | A | B | r | Max $NO_x EI$ |
|---|---|---|---|---|
| GT-309 (reverse flow effect neglected) | 2.583 | 1.104 | .8992 | ≃ 19 |
| GT-309 (reverse flow effect included) | 3.836 | 1.161 | .9548 | ≃ 19 |
| T-63 | 6.882 | 0.686 | .9223 | ≃ 10 |
| JT9D (swirl effect neglected) | 5.326 | -1.089 | .9502 | ≃ 46 |
| JT9D (swirl effect included) | 4.713 | -1.089 | .9502 | ≃ 46 |

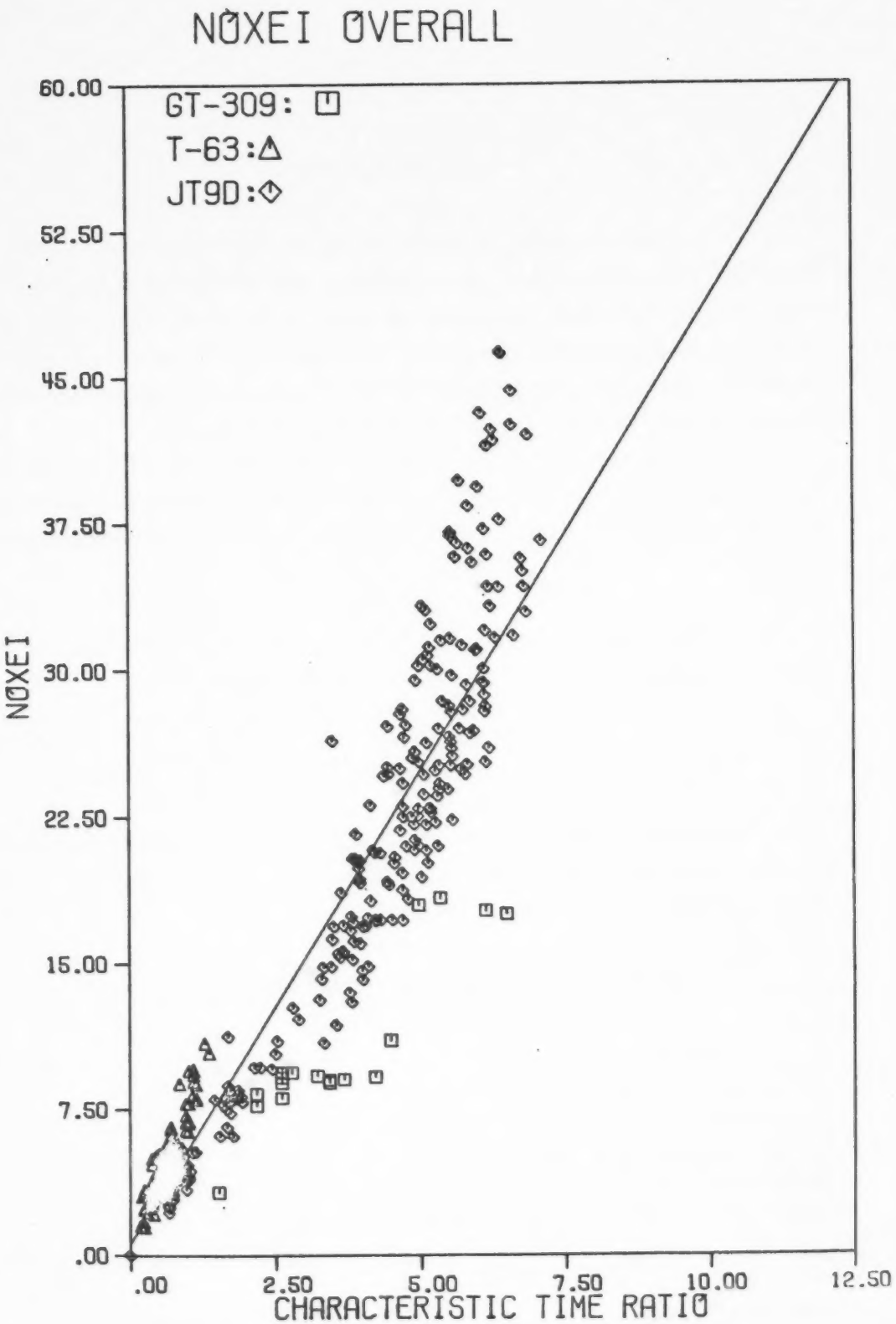


Figure 6-1. $NO_xEI$ correlation for three engines.

Notice that there are considerable variations in the slopes of the correlations. This is disturbing since a universal slope is being sought. Part of these variations may be due to the data existing over different ranges of emission values but this too is troublesome since a direct proportionality between $NO_x EI$ and $\tau_{s\ell,no}/\tau_{no}$ was derived in Section II.

Eq. 6-1 does indicate that including the reverse flow effect may improve the correlation. That is, the slope for the GT-309 is closer to the slope for the general correlation when the reverse flow effect is included. While it is true that the slopes for all of the engines would increase when reverse flow is included, and thus the slope for Eq. 6-1, the effect is strongest for the GT-309 because it has a larger percentage of the total flow entering at the assumed quench location than either the T-63 or the JT9D.

Likewise, Eq. 6-1 indicates that the swirl effect may have been properly accounted for. Notice that including the swirl brings the slope for the JT9D closer to the value for the general correlation.

In summary, the characteristic time model correlates nitric oxides for individual engines but these correlations may vary from engine to engine. However, it is noteworthy that the general correlation for the engines considered thus far is quite good (r = .9390).

## B. Carbon Monoxide

The combined COEI data for the GT-309, the T-63, and the JT9D were correlated; the least fit (shown in Fig. 6-2) is

$$COEI = 41.499\ \tau_{co}/\tau_{co,s\ell} + 0.959 \qquad 6\text{-}2$$

with r = .9138. This correlation consists of the data that assumes no swirl effect.

Table 6-2 shows the individual CO correlations.

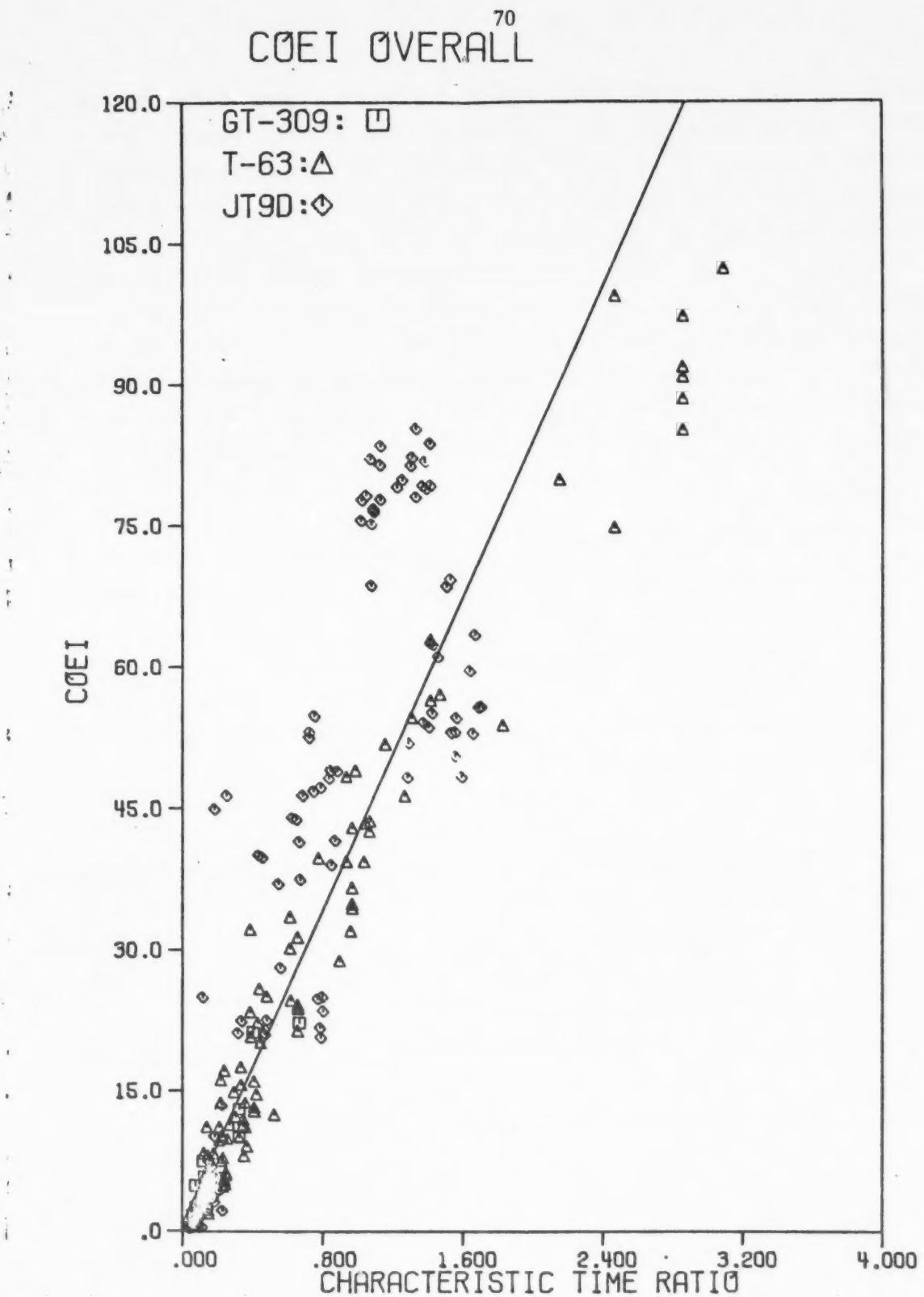


Figure 6-2. COEI correlation for three engines.

Table 6-2. Constants for COEI = $C\tau_{CO}/\tau_{s\ell,co} + D$

| Engine | C | D | r | Max COEI |
|---|---|---|---|---|
| GT-309 | 35.849 | 0.190 | .9440 | ≃ 22 |
| T-63 | 33.465 | 2.720 | .9742 | ≃100 |
| JT9D (swirl effect neglected) | 49.846 | -0.572 | .9301 | ≃ 86 |
| JT9D (swirl effect included) | 58.976 | -0.668 | .9310 | ≃ 86 |

Notice that, again, there are variations in the values of the slope but that the changes are not as great as some of those for the nitric oxide correlations. Also, the method of accounting of swirl seems to worsen the general CO correlation, perhaps because the liner wall (the assumed predominate region of CO oxidation quenching) may tend to interrupt the swirl pattern and cause there to be no swirl effect on CO.

## C. Summary

The characteristic time model correlates nitric oxides and carbon monoxide for the three combustors tested. The individual correlations differ substantially from the general correlations so there is some doubt about the universality of the overall results. Nevertheless, the general correlations were quite good.

In Section III, the utility of the characteristic time model as a design tool for optimizing emissions was demonstrated for the GT-309 automotive gas turbine combustor. Also, in Section V, the model was used to predict the effect of ambient conditions on nitric oxides.

## LIST OF REFERENCES

Blazowski, W. S. and Henderson, R. E. (1972). "Assessment of pollutant measurement and control technology and development of pollution reduction goals for military aircraft engines," AFAPL-TR-72-102.

Blazowski, W. S., Walsh, D. E. and Mach, K. D. (1975). "Operating and ambient condition influences on aircraft gas turbine $NO_x$ emissions," AIAA J. Aircraft 12, 110-115.

Carl, D. E. (1974). "Influence of ambient humidity on nitric oxide generation," Gas Turbine International 15 No. 3, 28-32.

Cornelius, W. (1976). Power Systems Department, General Motors Research Laboratories, Personal Communication.

Cornelius, W. and Wade, W. R. (1970). "The formation and control of nitric oxide in regenerative gas turbine burner," SAE Paper 700708.

Dodds, W. J., Colket, M. B. and Mellor, A. M. (1976). "Radiation and smoke from gas turbine flames. Part 1. Carbon particulate measurements within a model turbine combustor," USATACOM Tech. Rep. No. 12163, Part 1.

Environmental Protection Agency (1973). "Control of air pollution from aircraft and aircraft engines," U.S. Federal Register 38, (136) Part II, July 17.

Fenimore, C. P. (1970). "Formation of nitric oxide in premixed hydrocarbon flames," 373-380, Thirteen Symposium (International) on Combustion, The Combustion Institute, Pittsburgh.

Fredrikensen, H. P. (1972). In discussion of Wade and Cornelius (1972). Emissions from Continuous Systems, Plenum Press, N.Y.

Hammond, D. C., Jr. (1977). "Evaluation of characteristic time model emissions predictions for three GT-309 vehicular gas turbine combustors," AIAA J. Energy 1, 250-256.

Lipfert, F. W. (1972). "Correlation of gas turbine emissions data," ASME Paper 72-GT-60.

Mellor, A. M. (1972). "Current kinetic modeling techniques for continuous flow combustors," 23-53, Emissions from Continuous Combustion Systems, Plenum Press, N.Y.

Mellor, A. M. (1973). "Simplified physical model of spray combustion in a gas turbine engine," Comb. Sci. Tech. 8, 101-109.

Mellor, A. M. (1976). "Gas turbine engine pollution," 111-133, Progress in Energy and Combustion Science 1, Pergamon Press, Oxford.

Mellor, A. M. (1977a). "Characteristic time emissions correlations and sample optimization: the GT-309 gas turbine combustor," AIAA J. Energy 1, 244-249.

Mellor, A. M. (1977b). "Characteristic time emissions correlations: the T-63 helicopter gas turbine engine," AIAA J. Energy 1, 257-262.

Mellor, A. M., Anderson, R. D., Altenkirch, R. A. and Tuttle, J. H. (1972). "Emissions from and within an Allison J-33 combustor," Comb. Sci. Tech. 6, 169-176.

Moses, C. A. (1975). "Studies of fuel volatility effects on turbine combustor performance," presented at Joint Spring Meeting of Western and Central States Section of the Combustion Institute.

Moses, C. A. (1976). Southwest Research Institute, Personal communication to W. J. Dodds, Purdue University.

Mularz, E. J., Wear, J. D. and Verbulecz, P. W. (1975). "Exhaust pollutant emissions from swirl-can combustor module arrays at parametric test conditions," NASA Rep. TM X-3237.

Nelson, A. W. (1976). Pratt and Whitney Aircraft, Personal Communication to R. Munt, Environmental Protection Agency, 12 October.

Roberts, R., Aceto, L. D., Kollrack, R., Bonnell, J. M. and Teixeira, D. P. (1971). "An analytical model for nitric oxide formation in a gas turbine combustion chamber," AIAA Paper No. 71-715.

Sawyer, R. F., Cernansky, N. P. and Oppenheim, A. K. (1973). "Factors controlling pollutant emissions from gas turbine engines," Atmospheric Pollution by Aircraft Engines, AGARD CP No. 125.

Sturgess, G. (1978). Pratt and Whitney Aircraft, Personal Communication to R. M. Washam, Purdue University.

Troth, D. L., Verdouw, A. J. and Verkamp, F. J. (1973). "Investigation of aircraft gas turbine combustor having low mass emissions," USAAMRDL Tech. Rep. 73-6.

Troth, D. L., Verdouw, A. J., Williams, J. R. and Dodd, R. G. (1974). "Investigation of aircraft gas turbine combustors having low mass emissions," ASME Paper No. 74-GT-36.

Tuttle, J. H., Altenkirch, R. A. and Mellor, A. M. (1973). "Emissions from and within an Allison J-33 combustor. II. The effect of inlet air temperature," Comb. Sci. Tech. 7, 125-134.

Tuttle, J. H., Colket, M. B. and Mellor, A. M. (1976). "Characteristic time correlation of emissions from conventional aircraft type flames," Rep. No. PURDU-CL-76-05, School of Mech. Eng., Purdue Univ.

Tuttle, J. H., Colket, M. B., Bilger, R. W. and Mellor, A. M. (1977). "Characteristic times for combustion and pollutant formation in spray combustion," 209-219, Sixteenth Symposium (International) on Combustion, The Combustion Institute, Pittsburgh.

Vermes, G. (1974). "A $NO_x$ correlation method for gas turbine combustors based on $NO_x$ formation assumptions," ASME Paper 74-WA/GT-10.

Wade, W. R. and Cornelius, W. (1972). "Emissions characteristics of continuous combustion systems of vehicular powerplants-gas turbine, steam, Stirling," 375-450, Emissions from Continuous Combustion Systems, Plenum Press, N.Y.